

# Asynchronous Multiple Access in Optical Wireless Scattering Communication: Achievable Transmission Rates and Receiver Design

Guanchu Wang, Chen Gong, Zhimeng Jiang and Zhengyuan Xu

## Abstract

We investigate the asynchronous multiple user access communication in optical wireless scattering communication, where different users transmit signals without perfect alignment in the time domain. Firstly, we characterize the received signal based on hidden markov model (HMM) such that the misalignment among different users can be characterized by the state transition. Then, we investigate the achievable rates based on that of the HMM and obtain the approximated solution using Monte Carlo method. We propose the channel estimation based on expectation-maximization (EM) algorithm. Furthermore, we adopt Viterbi and Bahl-Cocke-Jelinek-Raviv (BCJR) algorithms for joint iterative multi-user decoding. Numerical and experimental results illustrate the performance of proposed channel estimation, joint detection and decoding. It is seen from the experimental results that the proposed approaches perform close to the simulation results.

## I. INTRODUCTION

Non-line of sight (NLOS) ultraviolet (UV) scattering communication serves as a good candidate for the applications where radio-silence is required and the transmitter-receiver alignment is hard to guarantee due to obstacles or the user mobility. Moreover, it is competent for outdoor communication under strong solar background because of negligible solar radiation in the UV spectrum [1]. Theoretical analysis [2], numerical simulation [3] and real experiments [4] imply extremely large path loss between the transmitter and receiver, where the received signal can be detected by the photon-counting receiver and characterized by Poisson distributed number of discrete photoelectrons.

This work was supported by Key Program of National Natural Science Foundation of China (Grant No. 61631018) and Key Research Program of Frontier Sciences of CAS (Grant No. QYZDY-SSW-JSC003).

The authors are with Key Laboratory of Wireless-Optical Communications, Chinese Academy of Sciences, School of Information Science and Technology, University of Science and Technology of China, Hefei, China. Email: {hegsns, zhimengj}@mail.ustc.edu.cn, {cgong821, xuzy}@ustc.edu.cn.

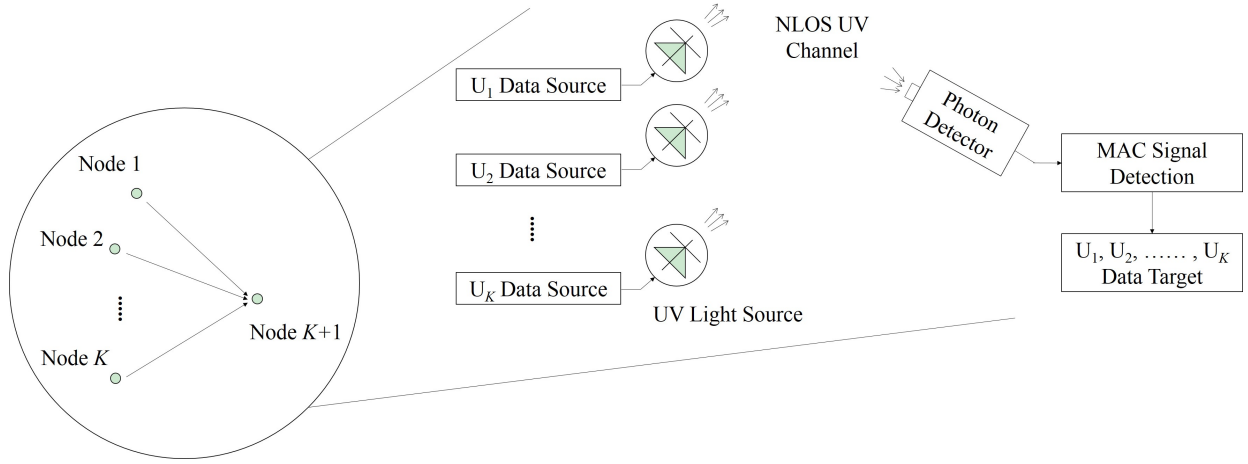


Fig. 1. Configuration of the asynchronous multiple access (AMA).

The capacity of point-to-point continuous-time Poisson channel has been investigated in [5]–[7] and the capacity of discrete-time aspect has been derived in [8], [9]. Moreover, the optimal source distribution for the discrete-time perspective has recently been studied in [10]. Besides point-to-point communication, multiuser scattering communication has been addressed in [11]–[13]. Note that in [14] code division and non-orthogonal multiple access for optical wireless scattering communication has been investigated, assuming one transmitter broadcasts to multiple receivers where the symbols for multiple receivers are perfectly aligned in the time domain. However, as shown in Figure 1, asynchronous multiple access (AMA) may happen for multiple users that independently transmit signals in a common channel in an ad-hoc network, where the transmitted symbols are not necessarily aligned in the time domain. Consequently, the signal characterization, achievable transmission rate, and signal detection for such asynchronous access communication network need to be investigated.

In this work, we characterize the asynchronous multiple access based on discrete Poisson channel, where the misalignment in the time domain among different users transmission is considered. Specifically, we adopt hidden markov model (HMM) [15]–[17] to characterize the asynchronous multiple access. Then, we conceive the achievable rates for multiple users and obtain the approximated solution based on Monte Carlo method. For the receiver-side signal processing, we propose channel estimation based on expectation-maximization (EM) algorithm [18], [19], and adopt Viterbi [20], [21] and Bahl-Cocke-Jelinek-Raviv (BCJR) [22], [23] algorithms for symbol detection, respectively. Furthermore, we propose iterative algorithm for the multi-user maximum-likelihood/maximum a posteriori probability (ML/MAP) joint decoding [24], [25]. Numerical results show the achievable sum rates, the performance behavior of channel estimation as well as ML/MAP joint detection and decoding with respect to the relative delay

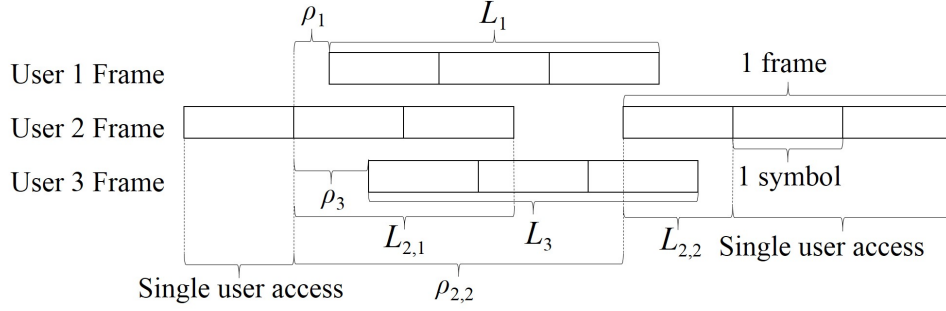


Fig. 2.  $((1, 2, 1), \{3, \{2, 1\}, 3\}, \{0.3, \{0, 3\}, 0.6\})$  AMA.

among different users. Finally, we conduct offline experiments to evaluate the performance of the proposed approaches. It is seen that based on the experimental measurements, the proposed approaches perform close to the simulation results with the identical channel parameters.

The remainder of the paper is organized as follows. In Section II, we characterize NLOS asynchronous multiple access scattering communication using the HMM. In Section III, we investigate the achievable transmission rates and obtain the approximated solution based on Monte Carlo method. In Section IV, we propose the channel estimation based on correlation maximization and EM algorithm. In Section V, we adopt Viterbi/BCJR algorithm and propose the iterative joint ML/MAP detection and decoding for the asynchronous multiple access communication system under consideration. The numerical and experimental results are given in Sections VI and VII, respectively. Finally, we conclude this paper in Section VIII.

## II. SYSTEM MODEL

### A. Discrete Poisson Asynchronous Multiple Access Channel

We consider NLOS scattering communication systems accessed by asynchronous multiple users, where each user deploys on-off key modulation. The asynchronous multiple access (AMA) is based on the fact that the transmitted symbols of different users are not necessarily aligned in the time domain due to the possible ad-hoc network deployment. We characterize the AMA by parameters  $\mathbf{M}_{\mathcal{K}} = \{M_k | k \in \mathcal{K}\}$ ,  $\mathbf{L}_{\mathcal{K}} = \{L_k | k \in \mathcal{K}\}$  and  $\mathbf{P}_{\mathcal{K}} = \{\rho_k | k \in \mathcal{K}\}$ , where  $\mathcal{K}$  denotes the set of all AMA users;  $M_k$ ,  $L_k = \{L_{k,i} | 1 \leq i \leq M_k\}$  and  $\rho_k = \{\rho_{k,i} | 1 \leq i \leq M_k\}$  denote the number of frames, the number of symbols and the start time of each frame for user  $k$ , respectively; and  $\rho_{k,i}$  is in the unit of symbol duration. The AMA with the above parameters is defined as  $(\mathbf{M}_{\mathcal{K}}, \mathbf{L}_{\mathcal{K}}, \mathbf{P}_{\mathcal{K}})$  AMA for short. Figure 2 illustrates the  $((1, 2, 1), \{3, \{2, 1\}, 3\}, \{0.3, \{0, 3\}, 0.6\})$  AMA, where the start of each symbol duration and the misalignment are marked.

We divide each symbol into several chips such that the misalignment of users' symbols can be characterized by the chip level. Let  $T_s$  and  $\mathbf{T}_c = \{\tau_t | 1 \leq t \leq T\}$  denote the symbol duration and chip

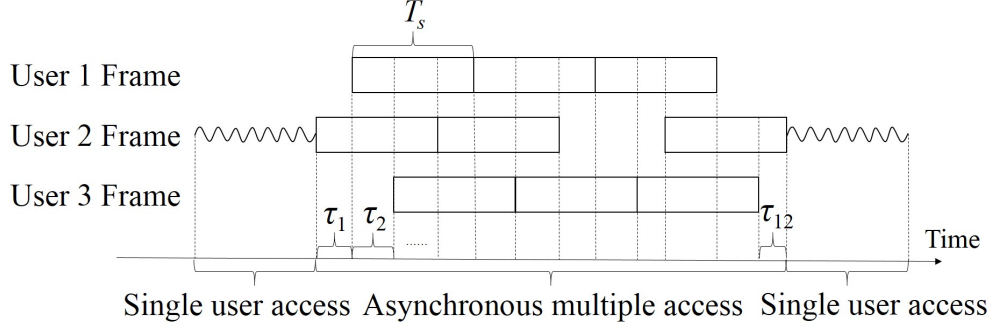


Fig. 3. Chip-level-characterization for AMA.

duration within the AMA, respectively, where  $\tau_t$  is in the unit of  $T_s$ ; and  $T$  denotes the total number of chips. The characterization of AMA in the chip level is illustrated in Figure 3. Furthermore, let  $\mathcal{K}_t$  and  $\mathbf{z}_{\mathcal{K}_t} = \{z_{t,k} | k \in \mathcal{K}_t\}$  denote the set of AMA users and their transmitted symbols in the  $t^{\text{th}}$  chip, respectively. Due to the weak received signal intensity of NLOS UV scattering communications, the received signal can be characterized by discrete photoelectrons, whose number satisfies a Poisson distribution. More specifically, let  $\lambda_0$  and  $\lambda_k$  denote the mean number of detected photoelectrons for the background radiation and user  $k$ . The number of detected photoelectrons  $N_t$  in the  $t^{\text{th}}$  chip for  $1 \leq t \leq T$  satisfies the following Poisson distribution

$$\mathbb{P}(N_t = n) = \frac{\tau_t^n}{n!} (\lambda_0 + \mathbf{\Lambda}_{\mathcal{K}_t} \cdot \mathbf{z}_{\mathcal{K}_t})^n e^{-\tau_t(\lambda_0 + \mathbf{\Lambda}_{\mathcal{K}_t} \cdot \mathbf{z}_{\mathcal{K}_t})}, \quad (1)$$

where  $\mathbf{\Lambda}_{\mathcal{K}_t} = \{\lambda_k | k \in \mathcal{K}_t\}$ ; and  $\mathbf{\Lambda}_{\mathcal{K}_t} \cdot \mathbf{z}_{\mathcal{K}_t} = \sum_{k \in \mathcal{K}_t} \lambda_k z_{t,k}$ .

For  $(\mathbf{M}_{\mathcal{K}}, \mathbf{L}_{\mathcal{K}}, \mathbf{P}_{\mathcal{K}})$  AMA, let  $\mathbf{U} = \{u_t | u_t \in \mathbf{P}'_{\mathcal{K}}, u_t < u_{t+1}, 1 \leq t \leq T\}$  denote the set of border times of chips in the AMA, where  $u_t$  and  $u_{t+1}$  denote the start and end time of the  $t^{\text{th}}$  chip for  $1 \leq t \leq T$ , respectively; and  $\mathbf{P}'_{\mathcal{K}} = \{\rho_{k,j} + i | 0 \leq i \leq L_{k,j}, 1 \leq j \leq M_k, k \in \mathcal{K}\}$ . The chip duration, the total number of chips and the set of users in the  $t^{\text{th}}$  chip are respectively given by

$$\begin{aligned} \mathbf{T}_c &= \{\tau_t = u_{t+1} - u_t | 1 \leq t \leq T\}, \\ T &= \sum_{k \in \mathcal{K}} \sum_{i=1}^{M_k} L_{k,i} + \sum_{k \in \mathcal{K}} M_k - 1, \\ \mathcal{K}_t &= \{k | \rho_{k,i} \leq u_t < \rho_{k,i} + L_{k,i}, 1 \leq i \leq M_k\}. \end{aligned} \quad (2)$$

### B. Hidden Markov Model for AMA

Note that due to the overlap of symbols for different users, the numbers of detected photoelectrons in different chips are correlated with each other. We deploy HMM to characterize AMA in the chip level. Let  $\mathbf{e}_{\mathcal{K}} = \{\mathbf{e}_k | k \in \mathcal{K}\}$  denote the set of orthogonal bases, where  $\mathbf{e}_k$  denotes the  $|\mathcal{K}|$ -dimensional vector

satisfying  $\mathbf{e}_i^T \cdot \mathbf{e}_i = 1$  and  $\mathbf{e}_i^T \cdot \mathbf{e}_j = 0$  for  $i \neq j \in \mathcal{K}$ , where  $|\mathcal{K}|$  denotes the number of elements in  $\mathcal{K}$ . We denote  $\mathbf{S}_T = \{\mathbf{S}_t | 1 \leq t \leq T\}$  and  $N_T = \{N_t | 1 \leq t \leq T\}$  as the state and observation sequence of the proposed HMM, where  $\mathbf{S}_t$  consists of the transmitted symbols of users in  $\mathcal{K}_t$  given by

$$\mathbf{S}_t = \sum_{k \in \mathcal{K}_t} z_{t,k} \mathbf{e}_k, \quad (3)$$

while the state space of the  $t$ th chip  $\mathcal{B}^{\mathcal{K}_t}$  is given by

$$\mathcal{B}^{\mathcal{K}_t} = \left\{ \sum_{k \in \mathcal{K}_t} \theta_k \mathbf{e}_k \mid \theta_k \in \{0, 1\}, k \in \mathcal{K}_t \right\}. \quad (4)$$

The HMM is determined by parameters  $(\boldsymbol{\pi}_0, \mathbf{A}_t, \mathbf{B}_t)$ , where  $\boldsymbol{\pi}_0$ ,  $\mathbf{A}_t$  and  $\mathbf{B}_t$  denote the initial distribution, state transition matrix and observation emission matrix, respectively. Note that the initial distribution is given by

$$\boldsymbol{\pi}_0 = \{\mathbb{P}(\mathbf{S}_1 = \mathbf{s}_{1,i}) \mid \mathbf{s}_{1,i} \in \mathcal{B}^{\mathcal{K}_1}\} = \left\{ \prod_{k \in \mathcal{K}_1} q_k^{s_{1,i} \cdot \mathbf{e}_k} (1 - q_k)^{1 - s_{1,i} \cdot \mathbf{e}_k} \mid \mathbf{s}_{1,i} \in \mathcal{B}^{\mathcal{K}_1} \right\}, \quad (5)$$

where  $q_k = \mathbb{P}(z_{t,k} = 1)$  for  $1 \leq t \leq T$ . The state transition matrix  $\mathbf{A}_t = [a_{t,i,j} | \mathbf{s}_{t,i} \in \mathcal{B}^{\mathcal{K}_t}, \mathbf{s}_{t+1,j} \in \mathcal{B}^{\mathcal{K}_{t+1}}]$ , where each element  $a_{i,j,t}$  is given by

$$a_{t,i,j} = \mathbb{P}(\mathbf{S}_{t+1} = \mathbf{s}_{t+1,j} | \mathbf{S}_t = \mathbf{s}_{t,i}) = \prod_{k \in \mathcal{K}_t \setminus \widetilde{\mathcal{K}}_{t+1}} (s_{t+1,j} \cdot \mathbf{e}_k) \odot (s_{t,i} \cdot \mathbf{e}_k) \prod_{k \in \widetilde{\mathcal{K}}_{t+1}} q_k^{s_{t+1,j} \cdot \mathbf{e}_k} (1 - q_k)^{1 - s_{t+1,j} \cdot \mathbf{e}_k}, \quad (6)$$

where  $\mathbf{s}_{t,i} \in \mathcal{B}^{\mathcal{K}_t}$  and  $\mathbf{s}_{t+1,j} \in \mathcal{B}^{\mathcal{K}_{t+1}}$  may take values among all possible choices of  $\mathbf{S}_t$  and  $\mathbf{S}_{t+1}$ , respectively;  $\odot$  indicates binary logical XNOR; and  $\widetilde{\mathcal{K}}_t = \{k | k \in \mathcal{K}_t, u_t - \rho_{k,i} \in \mathbb{N}, 1 \leq i \leq M_k\}$ . The observation emission matrix  $\mathbf{B}_t = [b_{t,i,n+1} | \mathbf{s}_{t,i} \in \mathcal{B}^{\mathcal{K}_t}, n \in \mathbb{N}]$ , where based on Equation (1) each element  $b_{i,n+1,t}$  is given by

$$b_{t,i,n+1} = \mathbb{P}(N_t = n | \mathbf{S}_t = \mathbf{s}_{t,i}) = \frac{\tau_t^n \lambda_{\mathbf{s}_{t,i}}^n}{n!} e^{-\tau_t \lambda_{\mathbf{s}_{t,i}}}, \quad (7)$$

where  $\lambda_{\mathbf{s}_{t,i}}$  is given by

$$\lambda_{\mathbf{s}_{t,i}} = \lambda_0 + \sum_{k \in \mathcal{K}_t} \lambda_k \mathbf{e}_k^T \mathbf{s}_{t,i}. \quad (8)$$

### III. HMM-BASED ACHIEVABLE TRANSMISSION RATE

We first provide the achievable rates for multiuser asynchronous multiple access, and then specify the results on the two-user multiple access channels.

### A. Achievable Rates for HMM

For notational simplicity but without loss of generality, we investigate the transmission rate for asynchronous Poisson channel accessed by fixed number of users, i.e.,  $\mathcal{K}_t = \mathcal{K}$  for  $1 \leq t \leq T$ . The achievable rates can be derived based on the mutual information between hidden states and observation sequences with finite chain length.

Let  $\mathbf{Z}_{\mathcal{K}} = \{\mathbf{Z}_k | k \in \mathcal{K}\}$  denote the transmission symbols of users in  $\mathcal{K}$ . Due to the statistical independence of transmitted symbols among the users, the expressions of entropy and conditional entropy of transmission symbols are given as follows

$$\begin{aligned} H(\mathbf{Z}_{\mathcal{K}}) &= \frac{T}{|\mathcal{K}|} \sum_{k \in \mathcal{K}} \mathcal{H}(q_k), \\ H(\mathbf{Z}_{\mathcal{U}} | \mathbf{Z}_{\mathcal{U}^c}) &= \frac{T}{|\mathcal{K}|} \sum_{k \in \mathcal{U}} \mathcal{H}(q_k), \end{aligned} \quad (9)$$

where  $\mathcal{B} = \{0, 1\}$ ;  $\mathcal{H}(q_k) = -q_k \log_2 q_k - (1 - q_k) \log_2 (1 - q_k)$ ;  $\mathcal{U}, \mathcal{U}^c \subset \mathcal{K}$ ;  $\mathcal{U} \cup \mathcal{U}^c = \mathcal{K}$ ; and  $\mathbf{Z}_{\mathcal{U}}$  and  $\mathbf{Z}_{\mathcal{U}^c}$  denote the transmission symbols of users in  $\mathcal{U}$  and  $\mathcal{U}^c$ , respectively.

The entropy and conditional entropy of transmission symbols given the observation sequences are given by

$$\begin{aligned} H(\mathbf{Z}_{\mathcal{K}} | \mathbf{N}_T) &= -\mathbb{E}_{\substack{\mathbf{z} \in \mathcal{B}^T \\ \mathbf{n} \in \mathbb{N}^T}} \left[ \log_2 \mathbb{P}(\mathbf{Z}_{\mathcal{K}} = \mathbf{z} | \mathbf{N}_T = \mathbf{n}) \right], \\ H(\mathbf{Z}_{\mathcal{U}} | \mathbf{Z}_{\mathcal{U}^c}, \mathbf{N}_T) &= -\mathbb{E}_{\substack{\mathbf{z} \in \mathcal{B}^T \\ \mathbf{n} \in \mathbb{N}^T}} \left[ \log_2 \mathbb{P}(\mathbf{Z}_{\mathcal{U}} = \mathbf{z}_{\mathcal{U}} | \mathbf{Z}_{\mathcal{U}^c} = \mathbf{z}_{\mathcal{U}^c}, \mathbf{N}_T = \mathbf{n}) \right], \end{aligned} \quad (10)$$

where  $\mathbb{N}$  denotes the set of natural number; and  $\mathbf{\Omega}^T$  denotes the  $T$ -time expansion of set  $\mathbf{\Omega}$ .

Note that for  $\forall \mathcal{U} \subseteq \mathcal{K}$ ,  $\mathcal{U} \neq \emptyset$ , the achievable sum rate of users in set  $\mathcal{U}$  must satisfy

$$\sum_{k \in \mathcal{U}} R_k \leq \frac{|\mathcal{K}|}{T} I(\mathbf{Z}_{\mathcal{U}}; \mathbf{N}_T | \mathbf{Z}_{\mathcal{U}^c}), \quad (11)$$

where  $R_k$  denotes the achievable rate of user  $k$ ;  $I(\mathbf{Z}_{\mathcal{U}}; \mathbf{N}_T | \mathbf{Z}_{\mathcal{U}^c})$  denotes the conditional mutual information given by

$$I(\mathbf{Z}_{\mathcal{U}}; \mathbf{N}_T | \mathbf{Z}_{\mathcal{U}^c}) = H(\mathbf{Z}_{\mathcal{U}} | \mathbf{Z}_{\mathcal{U}^c}) - H(\mathbf{Z}_{\mathcal{U}} | \mathbf{Z}_{\mathcal{U}^c}, \mathbf{N}_T). \quad (12)$$

Letting  $\mathcal{U} = \mathcal{K}$ , we have the following expression on the maximum achievable sum rate for all users,

$$R_{\Sigma} = \sup \sum_{k \in \mathcal{K}} R_k = \frac{1}{T} I(\mathbf{Z}_{\mathcal{K}}; \mathbf{N}_T). \quad (13)$$

### B. Low-complexity Solution for Achievable Rate

Note that the complexity of Equation (10) grows exponentially with the chain length  $T$ . Consequently, brute-force computation on the exact value of conditional entropy is intractable for large  $T$  due to

exhaustive enumeration of the state and observation sequences on  $\mathcal{B}^T$  and  $\mathbb{N}^T$ . The approximative solutions to  $H(\mathcal{Z}_{\mathcal{K}}|N_T)$  and  $H(\mathcal{Z}_{\mathcal{U}}|\mathcal{Z}_{\mathcal{U}^c}, N_T)$  are given by the following equations

$$\begin{aligned} H(\mathcal{Z}_{\mathcal{K}}|N_T) &\approx \mathbb{E}_{\substack{z \in \Psi_z \\ n \in \Psi_n}} \left[ H(\mathcal{Z}_{\mathcal{K}}|N_T = \mathbf{n}) \right], \\ H(\mathcal{Z}_{\mathcal{U}}|\mathcal{Z}_{\mathcal{U}^c}, N_T) &\approx \mathbb{E}_{\substack{z \in \Psi_z \\ n \in \Psi_n}} \left[ H(\mathcal{Z}_{\mathcal{U}}|\mathcal{Z}_{\mathcal{U}^c} = \mathbf{z}_{\mathcal{U}^c}, N_T = \mathbf{n}) \right], \end{aligned} \quad (14)$$

where  $\Psi_z \subset \mathcal{B}^T$  and  $\Psi_n \subset \mathbb{N}^T$  denote the set of samples on  $\mathcal{B}^T$  and  $\mathbb{N}^T$  with relatively high probability, respectively.

We resort to Monte Carlo method, which keeps generating random states and observation sequences based on the initial state distribution, the transition probability matrices, and the observation emission matrices. For each state and observation sequence realization, we have that

$$H(\mathcal{Z}_{\mathcal{K}}|N_T = \mathbf{n}) = H(\mathcal{S}_T|N_T = \mathbf{n}), \quad (15)$$

$$H(\mathcal{Z}_{\mathcal{U}}|\mathcal{Z}_{\mathcal{U}^c} = \mathbf{z}_{\mathcal{U}^c}, N_T = \mathbf{n}) = H(\mathcal{S}_T|\mathcal{Z}_{\mathcal{U}^c} = \mathbf{z}_{\mathcal{U}^c}, N_T = \mathbf{n}), \quad (16)$$

where efficient computation of the conditional entropy in Equation (15) can be conducted following [26].

To compute Equation (16), we define a new HMM with state sequence  $\tilde{\mathcal{S}}_T$  and observation sequence  $\tilde{N}_T$  depending on  $\mathcal{U}$  and  $\mathcal{U}^c$ , where the state space is given by

$$\mathcal{B}^{\mathcal{U}|\mathcal{U}^c} = \{\mathbf{s}_{t,i} | \forall k \in \mathcal{U}, \mathbf{s}_{t,i} \cdot \mathbf{e}_k \in \mathcal{B}^{\mathcal{U}}, \forall k \in \mathcal{U}^c, \mathbf{s}_{t,i} \cdot \mathbf{e}_k = z_{t,k}\}. \quad (17)$$

The initial distribution, state transition matrix and observation emission matrix  $(\tilde{\pi}_0, \tilde{A}_t, \tilde{B}_t)$  of the new HMM are respectively given by

$$\begin{aligned} \tilde{\pi}_0(i) &= \frac{\pi_0(i)}{\sum_{\mathbf{s}_{t,i} \in \mathcal{B}^{\mathcal{U}|\mathcal{U}^c}} \pi_0(i)}, \\ \tilde{b}_{t,i,n+1} &= \mathbb{P}(N_t = n | \tilde{\mathcal{S}}_t = \mathbf{s}_{t,i}) = b_{t,i,n+1}, \\ \tilde{a}_{t,i,j} &= \mathbb{P}(\tilde{\mathcal{S}}_{t+1} = \mathbf{s}_{t+1,j} | \tilde{\mathcal{S}}_t = \mathbf{s}_{t,i}) = \frac{a_{t,i,j}}{\sum_{j \in \mathcal{B}^{\mathcal{U}|\mathcal{U}^c}} a_{t,i,j}}, \end{aligned} \quad (18)$$

where  $\mathbf{s}_{t,i}, \mathbf{s}_{t,j} \in \mathcal{B}^{\mathcal{U}|\mathcal{U}^c}$ . We can hereby calculate Equation (16) according to the algorithm in [26] via the following transformation

$$H(\mathcal{S}_T|\mathcal{Z}_{\mathcal{U}^c} = \mathbf{z}_{\mathcal{U}^c}, N_T = \mathbf{n}) = H(\tilde{\mathcal{S}}_T|\tilde{N}_T = \mathbf{n}). \quad (19)$$

### C. Special Case for Two-user

For two-user AMA,  $\mathbf{P}_{\mathcal{K}}$  is simplified to the relative delay  $\rho$  between two users, where  $0 < \rho < 1$ . The achievable rates of two users must satisfy that

$$\begin{aligned} R_1 &\leq \frac{2}{T} \mathbb{I}(\mathbf{Z}_1; \mathbf{N}_T | \mathbf{Z}_2) = \mathcal{H}(q_1) - \frac{2}{T} \mathbb{H}(\mathbf{Z}_1 | \mathbf{Z}_2, \mathbf{N}_T), \\ R_2 &\leq \frac{2}{T} \mathbb{I}(\mathbf{Z}_2; \mathbf{N}_T | \mathbf{Z}_1) = \mathcal{H}(q_2) - \frac{2}{T} \mathbb{H}(\mathbf{Z}_2 | \mathbf{Z}_1, \mathbf{N}_T), \\ R_1 + R_2 &\leq \frac{2}{T} \mathbb{I}(\mathbf{Z}_1, \mathbf{Z}_2; \mathbf{N}_T) = \mathcal{H}(q_1) + \mathcal{H}(q_2) - \frac{2}{T} \mathbb{H}(\mathbf{Z}_1, \mathbf{Z}_2 | \mathbf{N}_T). \end{aligned} \quad (20)$$

We have the following propositions on  $\mathbb{H}(\mathbf{Z}_1 | \mathbf{Z}_2, \mathbf{N}_T)$ ,  $\mathbb{H}(\mathbf{Z}_2 | \mathbf{Z}_1, \mathbf{N}_T)$  and  $\mathbb{H}(\mathbf{Z}_1, \mathbf{Z}_2 | \mathbf{N}_T)$ .

**Proposition 1.** *The chain rules on conditional probabilities are given as follows*

$$\begin{aligned} \mathbb{P}(\mathbf{Z}_1 | \mathbf{Z}_2, \mathbf{N}_T) &= \prod_{t=1}^{\frac{T}{2}} \mathbb{P}(Z_{1,t} | Z_{2,t}, Z_{2,t+1}, N_{2t-1}, N_{2t}), \\ \mathbb{P}(\mathbf{Z}_2 | \mathbf{Z}_1, \mathbf{N}_T) &= \prod_{t=1}^{\frac{T}{2}} \mathbb{P}(Z_{2,t} | Z_{1,t}, Z_{1,t+1}, N_{2t-1}, N_{2t}). \end{aligned} \quad (21)$$

We give the Proof in Appendix A.

**Proposition 2.** *The two users' conditional entropies are given by*

$$\begin{aligned} \mathbb{H}(\mathbf{Z}_1 | \mathbf{Z}_2, \mathbf{N}_T) &= \frac{T}{2} \sum_{X, Y_1, Y_2 \in \mathcal{B}} \mathbb{P}(X) \mathbb{P}(Y_1) \mathbb{P}(Y_2) \sum_{N_1, N_2 \in \mathbb{N}} \mathbb{P}(N_1 | X, Y_1) \mathbb{P}(N_2 | X, Y_2) \log_2 \frac{\mathbb{P}(N_1 | X, Y_1) \mathbb{P}(N_2 | X, Y_2) \mathbb{P}(X)}{\sum_{X \in \mathcal{B}} \mathbb{P}(X) \mathbb{P}(N_1 | X, Y_1) \mathbb{P}(N_2 | X, Y_2)}, \\ \mathbb{H}(\mathbf{Z}_2 | \mathbf{Z}_1, \mathbf{N}_T) &= \frac{T}{2} \sum_{X_1, X_2, Y \in \mathcal{B}} \mathbb{P}(X_1) \mathbb{P}(X_2) \mathbb{P}(Y) \sum_{N_1, N_2 \in \mathbb{N}} \mathbb{P}(N_1 | X_1, Y) \mathbb{P}(N_2 | X_2, Y) \log_2 \frac{\mathbb{P}(N_1 | X_1, Y) \mathbb{P}(N_2 | X_2, Y) \mathbb{P}(Y)}{\sum_{Y \in \mathcal{B}} \mathbb{P}(Y) \mathbb{P}(N_1 | X_1, Y) \mathbb{P}(N_2 | X_2, Y)}, \end{aligned} \quad (22)$$

where  $\mathbb{P}(X) = q_1^X (1 - q_1)^{(1-X)}$ ,  $\mathbb{P}(Y) = q_2^Y (1 - q_2)^{(1-Y)}$ ; and

$$\begin{aligned} \mathbb{P}(N_1 | X, Y_1) &= \mathcal{P}[N_1 | \rho(\lambda_0 + X\lambda_1 + Y_1\lambda_2)], \\ \mathbb{P}(N_2 | X, Y_2) &= \mathcal{P}[N_2 | (1 - \rho)(\lambda_0 + X\lambda_1 + Y_2\lambda_2)], \\ \mathbb{P}(N_1 | X_1, Y) &= \mathcal{P}[N_1 | (1 - \rho)(\lambda_0 + X_1\lambda_1 + Y\lambda_2)], \\ \mathbb{P}(N_2 | X_2, Y) &= \mathcal{P}[N_2 | \rho(\lambda_0 + X_2\lambda_1 + Y\lambda_2)], \end{aligned} \quad (23)$$

where  $\mathcal{P}(N | \lambda)$  is the abbreviation of Poisson distribution given by  $\mathcal{P}(N | \lambda) = \frac{\lambda^N}{N!} e^{-\lambda}$ .

We give the Proof in Appendix B.

**Proposition 3.** *Note that  $\mathbb{H}(\mathbf{Z}_1 | \mathbf{Z}_2, \mathbf{N}_T)$ ,  $\mathbb{H}(\mathbf{Z}_2 | \mathbf{Z}_1, \mathbf{N}_T)$  and  $\mathbb{H}(\mathbf{Z}_1, \mathbf{Z}_2 | \mathbf{N}_T)$  vary with  $\rho$ , denoted function  $\mathbb{H}(\rho)$ . We have that  $\mathbb{H}(\rho) = \mathbb{H}(1 - \rho)$  for  $0 \leq \rho \leq 1$ .*

*Proof:* The values of Equation (22) hold invariant, if we let  $\rho$  in Equation (23) take value of  $(1 - \rho)$ . The joint probability density function for observation and sate sequence  $\mathbb{P}(\mathbf{N}_T, \mathbf{S}_T, \rho)$  is given as follow,

$$\begin{aligned} & \mathbb{P}(\mathbf{N}_T, \mathbf{S}_T, \rho) \\ &= \mathbb{P}(\mathbf{S}_1)\mathbb{P}(\mathbf{S}_2|\mathbf{S}_1)\frac{\lambda_{\mathbf{S}_1}^{n_1}\lambda_{\mathbf{S}_2}^{n_2}}{n_1!n_2!}\prod_{t=2}^{\frac{T}{2}}\frac{\lambda_{\mathbf{S}_{2t}}^{n_{2t}}\lambda_{\mathbf{S}_{2t-1}}^{n_{2t-1}}}{n_{2t}!n_{2t-1}!}\mathbb{P}(\mathbf{S}_{2t}|\mathbf{S}_{2t-1})\mathbb{P}(\mathbf{S}_{2t-1}|\mathbf{S}_{2t-2})\prod_{t=1}^{\frac{T}{2}}\rho^{n_{2t-1}}(1-\rho)^{n_{2t}}e^{-\sum_{t=1}^{\frac{T}{2}}\rho\lambda_{\mathbf{S}_{2t-1}}+(1-\rho)\lambda_{\mathbf{S}_{2t}}}, \end{aligned} \quad (24)$$

and  $\mathbb{H}(\mathbf{Z}_1, \mathbf{Z}_2|\mathbf{N}_T)$  is hereby given by

$$\mathbb{H}(\mathbf{Z}_1, \mathbf{Z}_2|\mathbf{N}_T) = \sum_{\mathbf{N}_T \in \mathbb{N}^T} \sum_{\mathbb{S}} \mathbb{P}(\mathbf{N}_T, \mathbf{S}_T, \rho) \log_2 \frac{\mathbb{P}(\mathbf{N}_T, \mathbf{S}_T, \rho)}{\sum_{\mathbb{S}} \mathbb{P}(\mathbf{N}_T, \mathbf{S}_T, \rho)}, \quad (25)$$

where  $\mathbb{S}$  is the abbreviation of  $\mathbf{S}_t \in \mathcal{B}^{\mathcal{K}_t}$  for  $1 \leq t \leq T$ .

Let  $\tilde{\Omega} = \{\tilde{\omega}_t | 1 \leq t \leq \frac{T}{2}\}$  denote a map for set  $\Omega = \{\omega_t | 1 \leq t \leq \frac{T}{2}\}$ , where we have  $\tilde{\omega}_{2t} = \omega_{2t-1}$  and  $\tilde{\omega}_{2t-1} = \omega_{2t}$  for  $1 \leq t \leq \frac{T}{2}$ . We have that  $\mathbb{P}(\mathbf{N}_T, \mathbf{S}_T, 1 - \rho) = \mathbb{P}(\tilde{\mathbf{N}}_T, \tilde{\mathbf{S}}_T, \rho)$ .  $\square$

#### IV. HMM-BASED CHANNEL ESTIMATION

The channel estimation involves the estimation of parameters  $(\mathbf{M}_{\mathcal{K}}, \mathbf{L}_{\mathcal{K}}, \mathbf{P}_{\mathcal{K}})$  and the mean number of detected photoelectrons  $\Lambda_T = \{\Lambda_t | 1 \leq t \leq T\}$ , where  $\Lambda_t = \{\lambda_{s_{t,i}} | s_{t,i} \in \mathcal{B}^{\mathcal{K}_t}\}$  denotes the mean value of all states in the  $t$ th chip of AMA. We propose a two-step estimation approach based on the pilot sequence at the beginning of each frame, where  $(\mathbf{M}_{\mathcal{K}}, \mathbf{L}_{\mathcal{K}}, \mathbf{P}_{\mathcal{K}})$  and  $\Lambda_T$  are estimated based on the correlation maximization and EM algorithm, respectively.

##### A. Correlation-based Estimation of $(\mathbf{M}_{\mathcal{K}}, \mathbf{L}_{\mathcal{K}}, \mathbf{P}_{\mathcal{K}})$

The frame detection can be performed via computing the correlation between the pilot sequence and searching the correlation peaks, which is presented in [27] in detail. More specifically, let  $C_k$  denote the correlation value for user  $k$ ,  $k \in \mathcal{K}$ , where the peak value implies the beginning of each frame for user  $k$ . The AMA detection is performed based on the fact that the interval between two consecutive peaks is shorter than the preset frame duration, as shown in Figure 4.

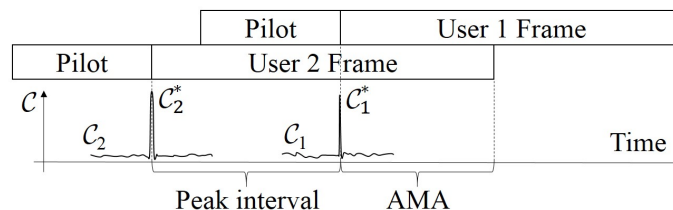


Fig. 4. Illustration for the AMA detection.

Consequently,  $\mathbf{M}_{\mathcal{K}}$  equals the number of correlation peaks for each user;  $\mathbf{L}_{\mathcal{K}}$  is implied by the number of symbols between the correlation peaks and the frame termination for each user; and  $\mathbf{P}_{\mathcal{K}}$  can be estimated via computing the interval between the AMA start time and correlation peaks for each user.

### B. EM Algorithm-based Estimation of $\Lambda_T$

Since the pilot sequence of different users may not be aligned, satisfactory estimation for the intensity of one user may require the detection of overlapping symbols from other users. We adopt EM algorithm for the estimation of  $\Lambda_T$ , and refine the estimation result when any user has finished transmitting the pilot sequence. Since  $\mathcal{K}_t$  is invariant during the estimation, we simplify  $\mathcal{K}_t$  and  $s_{t,i}$  into  $\mathcal{K}'$  and  $s_i$ , respectively.

We divide each chip into  $W$  sub-chips uniformly, where photon-counting is performed in each sub-chip. Let  $N_t = \{N_{t,m} | 1 \leq m \leq W\}$ , where  $N_{t,m}$  denotes the number of detection photoelectrons in the  $m$ th sub-chip of the  $t$ th chip. The updating rule for EM algorithm is proposed as follows.

**The E-step:** In the  $v$ th iteration, based on the estimate result  $\hat{\lambda}_{s_i}^{(v-1)}$  in the  $(v-1)$ th iteration, a posterior probability of  $S_t$  is given by

$$Q^{(v)}(S_t = s_i) = \mathbb{P}(S_t = s_i | N_t, \lambda_{s_i} = \hat{\lambda}_{s_i}^{(v-1)}) = \frac{\mathbb{P}(N_t, S_t = s_i | \lambda_{s_i} = \hat{\lambda}_{s_i}^{(v-1)})}{\sum_{s_i \in \mathcal{B}^{\mathcal{K}'}} \mathbb{P}(N_t, S_t = s_i | \lambda_{s_i} = \hat{\lambda}_{s_i}^{(v-1)})}, \quad (26)$$

where

$$\mathbb{P}(N_t, S_t = s_i | \lambda_{s_i} = \hat{\lambda}_{s_i}^{(v-1)}) = \prod_{m=1}^W \frac{[\tau_t \hat{\lambda}_{s_i}^{(v-1)}]^{N_{t,m}}}{W^{N_{t,m}} N_{t,m}!} e^{-\frac{\tau_t \hat{\lambda}_{s_i}^{(v-1)}}{W}}. \quad (27)$$

**The M-step:** Given a posterior probability  $Q^{(v)}(S_t = s_i)$  for the  $v$ th iteration, the ML-estimation for  $\hat{\Lambda}_T^{(v)} = \{\hat{\lambda}_{s_i}^{(v)} | s_i \in \mathcal{B}^{\mathcal{K}'}\}$  is given by

$$\hat{\lambda}_{s_i}^{(v)} = \frac{\sum_{t=1}^{T'} Q^{(v)}(S_t = s_i) \sum_{m=1}^W N_{t,m}}{\sum_{t=1}^{T'} Q^{(v)}(S_t = s_i) \tau_t}, \quad (28)$$

where  $T'$  denotes the number of chips within the pilot sequence; and the preset initial  $\hat{\Lambda}_T^{(0)}$  must satisfy  $\hat{\lambda}_{s_i}^{(0)} \neq \hat{\lambda}_{s_j}^{(0)} \neq 0$  for  $i \neq j$ . We give the proofs of M-step and the convergency of estimation in Appendix C.

## V. HMM-BASED SYMBOL DETECTION

Based on the proposed HMM, the receiver aims to detect the state sequence  $\mathbf{S}_T$  according to the observation sequence  $N_T$ . For joint detection and decoding, the Viterbi and BCJR algorithms are adopted to maximize the likelihood function  $\mathbb{P}(N_T | \mathbf{S}_T = \mathbf{s})$  and a posteriori probability  $\mathbb{P}(\mathbf{Z}_T = \mathbf{z} | N_T)$ , respectively, hence minimizes the error rate of sequence and symbol detection, respectively. Since the band-pass

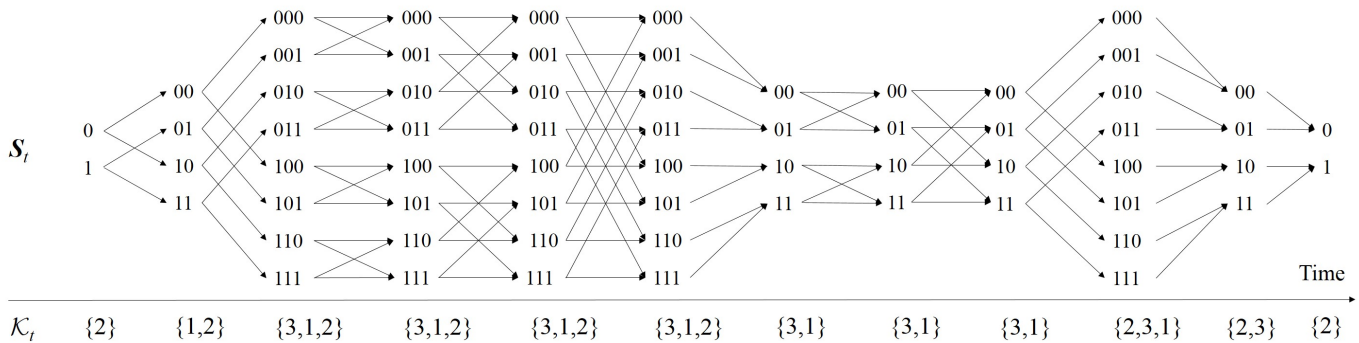


Fig. 5. Trellis diagram for  $((1, 2, 1), \{3, \{2, 1\}, 3\}, \{0.3, \{0, 3\}, 0.6\})$  AMA.

characteristic of LED, inter-symbol interference and error correcting code as well as other factors can cause the correlation among the received symbols, BCJR always behaves better than Viterbi algorithm while with higher computational complexity.

For both Viterbi and BCJR algorithms, the trellis diagram for the time-varying HMM is adapted to find the optimal state transition path maximizing the likelihood function or a posteriori probability. Figure 5 illustrates the trellis diagram for the HMM based on  $((1, 2, 1), \{3, \{2, 1\}, 3\}, \{0.3, \{0, 3\}, 0.6\})$  AMA, where each state  $\mathcal{S}_t$  is simplified to  $\{z_{k,t} | k \in \mathcal{K}_t\}$  in expression, and each branch between adjacent states corresponds to a non-zero element of  $\mathbf{A}_t$ .

#### A. Viterbi Algorithm-Based ML Detection

For the Viterbi algorithm, we maximize the log-likelihood function of state sequence summarized as follows

$$\hat{\mathbf{S}}_T = \arg \max_{\mathbf{S}_t \in \mathcal{B}^{\mathcal{K}_t}} \sum_{t=1}^T N_t \log \tau_t \lambda_{\mathbf{S}_t} - \tau_t \lambda_{\mathbf{S}_t}, \quad (29)$$

where  $\lambda_{\mathbf{S}_t}$  is computed by Equation (8) for  $\mathbf{S}_t \in \mathcal{B}^{\mathcal{K}_t}$ .

Letting  $\mathcal{L}(N_t | \mathbf{S}_t) = N_t \log \tau_t \lambda_{\mathbf{S}_t} - \tau_t \lambda_{\mathbf{S}_t}$ , we have that  $\mathcal{L}(N_t | \mathbf{S}_t) = \mathcal{L}(N_t | \mathbf{S}_t) + \mathcal{L}(N_{t-1} | \mathbf{S}_{t-1})$  for  $2 \leq t \leq T$ . Thus the dynamic programming is adopted with the following updated equation

$$\max \mathcal{L}(N_{t+1} | \mathbf{S}_t, \mathbf{S}_{t+1,j}) = \mathcal{L}(N_{t+1} | \mathbf{S}_{t+1,j}) + \max_{a_{i,j,t} \neq 0} \{\mathcal{L}(N_t | \mathbf{S}^{t-1}, \mathbf{S}_{t,i})\}, \quad (30)$$

where the initial solution is given by  $\mathcal{L}(N_1 | \mathbf{S}_1) = \mathcal{L}(N_1, \mathbf{S}_1)$ . The detected symbol sequence can be retrieved via tracing back the optimal path.

### B. BCJR Algorithm-Based MAP Detection

Letting  $z_{k,i,j} \in \mathbf{Z}_k$  denote the  $j$ th symbol in  $i$ th frame of user  $k$ , we maximize the posterior probability as follows

$$\hat{z}_{k,i,j} = \arg \max \log \mathbb{P}(z_{k,i,j} | \mathbf{N}_T) = \arg \max \log \mathbb{P}(\mathbf{S}_{z_{k,i,j}} | \mathbf{N}_T) \sim \arg \max \log \mathbb{P}(\mathbf{S}_{z_{k,i,j}}, \mathbf{N}_T), \quad (31)$$

where  $\mathbf{S}_{z_{k,i,j}}$  denotes the state sequence involving  $z_{k,i,j}$  from Equation (3).

To obtain  $\mathbb{P}(\mathbf{S}_{z_{k,i,j}}, \mathbf{N}_T)$ , we define the following probability functions

$$\begin{aligned} \alpha_t(\mathbf{s}) &= \mathbb{P}(\mathbf{S}_t = \mathbf{s}, \mathbf{N}_t), \\ \beta_t(\mathbf{s}) &= \mathbb{P}(\mathbf{N}_{[t+1,T]} | \mathbf{S}_t = \mathbf{s}), \\ \gamma_t(\mathbf{v}, \mathbf{s}) &= \mathbb{P}(\mathbf{N}_t, \mathbf{S}_t = \mathbf{s} | \mathbf{S}_{t-1} = \mathbf{v}), \end{aligned} \quad (32)$$

where  $N_{[a,b]} = \{N_t | a \leq t \leq b\}$ . Note that we have

$$\mathbb{P}(\mathbf{S}_{z_{k,i,j}} = \mathbf{\$}, \mathbf{N}_T) = \alpha_{\hat{t}_{k,i,j}}(\mathbf{s}_{\hat{t}_{k,i,j}}) \beta_{\hat{t}_{k,i,j}}(\mathbf{s}_{\hat{t}_{k,i,j}}) \prod_{t=\hat{t}_{k,i,j}}^{\hat{t}_{k,i,j}-1} \gamma_t(\mathbf{s}_t, \mathbf{s}_{t+1}), \quad (33)$$

where  $\mathbf{\$} = \{\mathbf{s}_t | \hat{t}_{k,i,j} \leq t \leq \hat{t}_{k,i,j}\}$ ; and  $\hat{t}_{k,i,j}$  and  $\hat{t}_{k,i,j}$  denote the first and last chip time instants involving  $z_{k,i,j}$ , respectively. Note that  $\gamma_t(\mathbf{s}_{t-1,i}, \mathbf{s}_{t,j}, n) = a_{i,j,t-1} b_{j,n+1,t}$  for  $\mathbf{s}_{t-1,i} \in \mathcal{B}^{\mathcal{K}_{t-1}}$ ,  $\mathbf{s}_{t,j} \in \mathcal{B}^{\mathcal{K}_t}$  and  $n \in \mathbb{N}$ . Then the calculations of  $\alpha(\mathbf{s}_t, \mathbf{n}')$  and  $\beta(\mathbf{s}_t, \mathbf{n}_{t+1}^T)$  are conducted according to the following recursive equations

$$\begin{aligned} \alpha_t(\mathbf{s}_t) &= \sum_{\mathbf{s}_{t-1} \in \mathcal{B}^{\mathcal{K}_{t-1}}} \alpha(\mathbf{s}_{t-1}) \gamma_t(\mathbf{s}_{t-1}, \mathbf{s}_t), \\ \beta_t(\mathbf{s}_t) &= \sum_{\mathbf{s}_{t+1} \in \mathcal{B}^{\mathcal{K}_{t+1}}} \beta_{t+1}(\mathbf{s}_{t+1}) \gamma_{t+1}(\mathbf{s}_t, \mathbf{s}_{t+1}). \end{aligned} \quad (34)$$

The initial values are  $\alpha_1(\mathbf{s}_{1,i}) = \boldsymbol{\pi}_0(\mathbf{s}_{1,i}) b_{i,N_1+1,1}$  for  $\mathbf{s}_{1,i} \in \mathcal{B}^{\mathcal{K}_1}$  and  $\beta_T(\mathbf{s}_T) = \boldsymbol{\pi}_{T-1}(\mathbf{s}_T)$  for  $\mathbf{s}_T \in \mathcal{B}^{\mathcal{K}_T}$ , where  $\boldsymbol{\pi}_0$  is given by Equation (5), and  $\boldsymbol{\pi}_t(\mathbf{s}_{t+1,i}) = \mathbb{P}(\mathbf{S}_{t+1} = \mathbf{s}_{t+1,i})$  is computed by the following recursive equation

$$\boldsymbol{\pi}_t(\mathbf{s}_{t+1,i}) = \sum_{\mathbf{s}_{t,j} \in \mathcal{B}^{\mathcal{K}_t}} a_{t,j,i} \boldsymbol{\pi}_{t-1}(\mathbf{s}_{t,j}). \quad (35)$$

### C. Joint Detection and Decoding

Based on the turbo processing, we propose the joint detection and decoding algorithm. For ML and MAP decoding, the log-likelihood ratio (*LLR*) and log-posterior ratio (*LAR*) are adopted as the input soft information for iteration, respectively. Let  $LLR_{z_{k,i,j}}^{(v)}$  and  $LAR_{z_{k,i,j}}^{(v)}$  denote the log-likelihood ratio and log-

aposterior-ratio of  $z_{k,i,j}$  after the  $v^{\text{th}}$  iteration, respectively. Typically each iteration of the turbo processing consists of one-time ML/MAP symbol detection followed by several channel decoding iterations.

For the ML-decoding, the initial  $LLR$  values are obtained by Viterbi algorithm

$$LLR_{z_{k,i,j}}^{(0)} = \log \frac{\mathbb{P}(N_T | z_{k,i,j} = 1)}{\mathbb{P}(N_T | z_{k,i,j} = 0)} = \sum_{t=\hat{i}_{k,i,j}}^{\hat{i}_{k,i,j}} \log \frac{\mathbb{P}(N_t | z_{t,k} = 1)}{\mathbb{P}(N_t | z_{t,k} = 0)}, \quad (36)$$

and the input  $LLR$  for the  $v^{\text{th}}$  iteration is given by

$$LLR_{z_{k,i,j}}^{(v-1)} = \log \frac{\mathbb{P}(N_T | z_{k,i,j} = 1)}{\mathbb{P}(N_T | z_{k,i,j} = 0)} = \sum_{t=\hat{i}_{k,i,j}}^{\hat{i}_{k,i,j}} \log \frac{\mathbb{E}_{s_t \in \mathcal{S}_{z_{k,t}}^1} \mathbb{P}(N_t | \mathbf{S}_t = s_t)}{\mathbb{E}_{s_t \in \mathcal{S}_{z_{k,t}}^0} \mathbb{P}(N_t | \mathbf{S}_t = s_t)}, \quad (37)$$

where  $\mathcal{S}_{z_{k,t}}^\theta = \{s_t | s_t^T \cdot \mathbf{e}_k = \theta\}$  for  $\theta \in \{0, 1\}$ ; and the expectation  $\mathbb{E}_{s_t \in \mathcal{S}_{z_{k,t}}^\theta} [\bullet]$  is calculated based on a posterior probabilities by the  $(v-1)$ th iteration of users in  $\mathcal{K}_t \setminus k$  as follows

$$\mathbb{E}_{s_t \in \mathcal{S}_{z_{k,t}}^\theta} [\bullet] = \sum_{s_t \in \mathcal{S}_{z_{k,t}}^\theta} \prod_{k' \in \mathcal{K}_t \setminus k} \mathbb{P}_{(v-1)}^{1-z_{t,k'}}(z_{k',t} = 0 | N_t) \mathbb{P}_{(v-1)}^{z_{t,k'}}(z_{k',t} = 1 | N_t) [\bullet], \quad (38)$$

where  $z_{t,k'} = s_t^T \cdot \mathbf{e}_{k'}$ ; and the a posterior probability of  $z_{k',t}$  after the  $(v-1)^{\text{th}}$  iteration is given by

$$\mathbb{P}_{(v-1)}(z_{t,k'} = 0 | N_t) = 1 - \mathbb{P}_{(v-1)}(z_{t,k'} = 1 | N_t) = \frac{1}{1 + e^{\frac{q_k}{1-q_k} J_{t,k'}^{(v-1)}}}, \quad (39)$$

where  $J_{t,k'}^{(v-1)} = \log \frac{\mathbb{P}_{(v-1)}(N_t | z_{t,k'} = 1)}{\mathbb{P}_{(v-1)}(N_t | z_{t,k'} = 0)}$  denotes the output  $LLR$  for  $z_{k',t}$  after the  $(v-1)^{\text{th}}$  iteration.

For MAP-decoding, the initial  $LAR$  is determined by BCJR detection as follows

$$LAR_{z_{k,i,j}}^{(0)} = \log \frac{\mathbb{P}(z_{k,i,j} = 1 | N_T)}{\mathbb{P}(z_{k,i,j} = 0 | N_T)}; \quad (40)$$

and the input  $LAR$  for the  $(v-1)^{\text{th}}$  iteration is given by

$$LAR_{z_{k,i,j}}^{(v-1)} = \log \frac{\mathbb{P}(N_T | z_{k,i,j} = 1)}{\mathbb{P}(N_T | z_{k,i,j} = 0)} + \log \frac{\mathbb{P}(z_{k,i,j} = 1)}{\mathbb{P}(z_{k,i,j} = 0)} = LLR_{z_{k,i,j}}^{(v-1)} + \log \frac{q_k}{1 - q_k}, \quad (41)$$

where  $LLR_{z_{k,i,j}}^{(v-1)}$  is computed according to Equations (37) and (38). Furthermore, the a posterior probability of MAP-decoding is given by

$$\mathbb{P}_{(v-1)}(z_{t,k'} = 0 | N_t) = 1 - \mathbb{P}_{(v-1)}(z_{t,k'} = 1 | N_t) = \frac{1}{1 + e^{J_{t,k'}^{(v-1)}}}, \quad (42)$$

where  $J_{t,k'}^{(v-1)} = \log \frac{\mathbb{P}_{(v-1)}(z_{t,k'} = 1 | N_t)}{\mathbb{P}_{(v-1)}(z_{t,k'} = 0 | N_t)}$  denotes the output  $LAR$  for  $z_{k',t}$  after the  $(v-1)^{\text{th}}$  iteration.

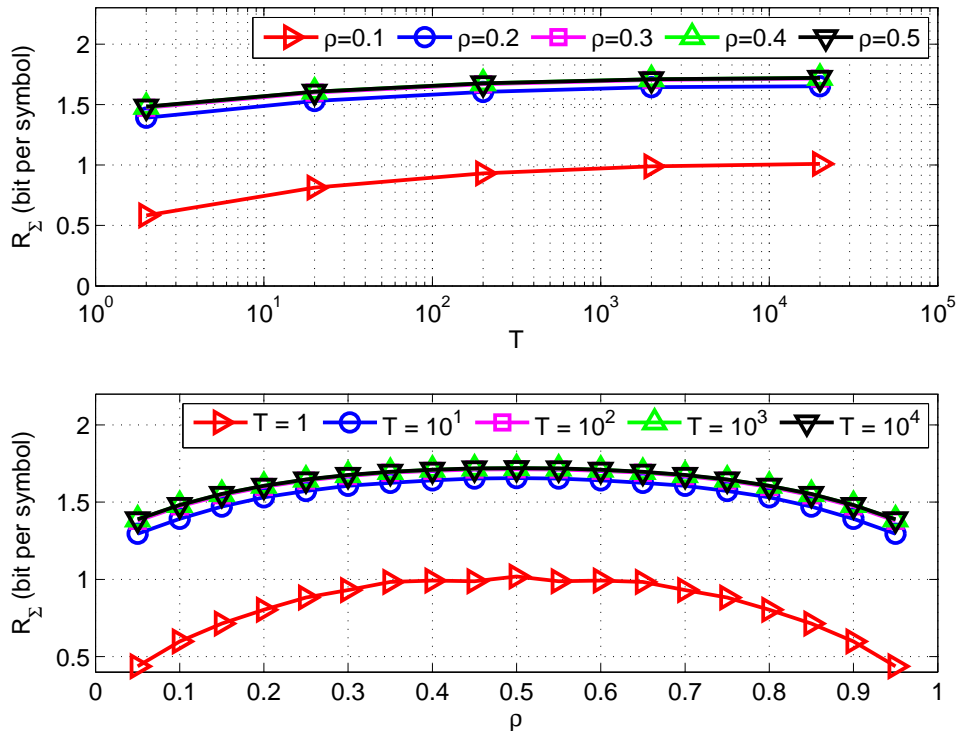


Fig. 6. The achievable sum rate for different  $\lambda_1$ ,  $\lambda_2$  and  $\rho$ .

## VI. SIMULATION RESULTS

### A. Achievable Rates for Spacial Case: Two Users

We consider two-user NLOS scattering AMA system in Section III.C. Figure 6 plots the achievable sum rate  $R_\Sigma$  versus the Markov chain length  $T$  for  $\lambda_1 = \lambda_2 = 10$  and  $\rho = 0.1, 0.2, 0.3, 0.4$  and  $0.5$ . It is seen that  $R_\Sigma$  grows with  $T$  and converges for  $T > 1 \times 10^3$ . Figure 7 illustrates  $R_\Sigma$  versus  $\lambda_1$  and  $\lambda_2$ , where the value of  $R_\Sigma$  is reflected by the color. It is seen that  $R_\Sigma$  decreases with  $\rho$  for  $\lambda_1 \gg \lambda_2$  or  $\lambda_1 \ll \lambda_2$ ; otherwise  $R_\Sigma$  increases with  $\rho$  closed to  $0.5$  for  $\lambda_1 \approx \lambda_2$ , where  $\lambda_1$  and  $\lambda_2$  affect  $R_\Sigma$  symmetrically.

### B. Simulation for Joint Detection and Decoding

We consider the NLOS scattering AMA system based on two cases: 2 users and 3 users. For the purpose of notational simplicity but without loss of generality, we assume  $M_k = 1$  for  $k = 1, 2$  and  $k = 1, 2, 3$ , while letting different users' frames completely overlap with each other, where subscript  $\bullet_{k,1}$  is simplified into  $\bullet_k$ . Other parameters  $\lambda_k = \lambda_{ave}$ ,  $q_k = 0.5$  and  $L_k = 12620$  are assumed for both  $k = 1, 2$  and  $k = 1, 2, 3$ .

Figure 8 illustrates the symbol error rate of ML and MAP detection versus  $\lambda_{ave}$  for the background radiation intensity  $\lambda_0 = 0.01$ . For the simulation of joint detection and decoding, we adopt a (12620, 6310) LDPC code for multi-users, where the parity check matrix construction and low-complexity message pass

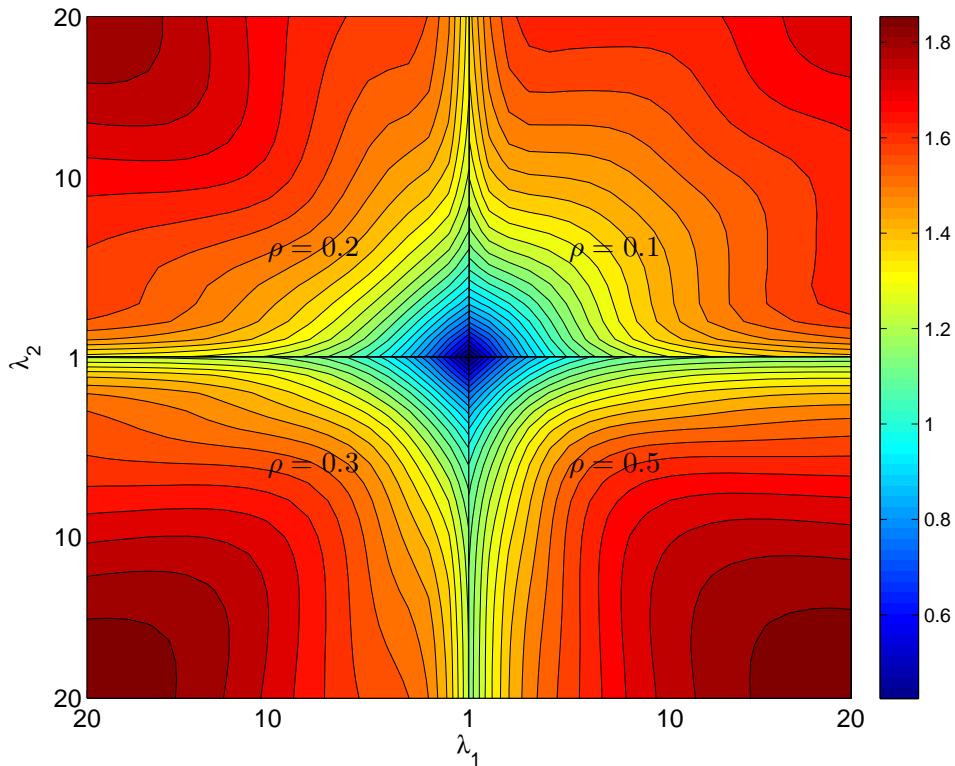


Fig. 7. The achievable sum rate versus  $\lambda_1$  and  $\lambda_2$  with respect of  $\rho$ .

decoding follow [28], [29] and [30]. The simulated bit error rates for ML and MAP joint decoding versus  $\lambda_{ave}$  are shown in Figure 9. It is observed that the existence of correlation among different symbols in a frame may lead to the performance gain of MAP detection/decoding over the ML detection/decoding. Moreover, with identical receiver side SNR of 2-user and 3-user AMA,  $\rho = 0.5$  and  $\rho_2 = \frac{1}{3}, \rho_3 = \frac{2}{3}$  can minimize the detection error probability, respectively.

## VII. EXPERIMENTAL RESULTS FOR SPECIAL CASE: TWO USERS

We conduct offline experiments on the performance of two-user AMA scattering UV communication to evaluate the proposed joint detection and decoding. At the transmitter side, two independent random bit streams drive the waveform generators to produce OOK signals. The Bias-Tees are employed to combine the AC and DC signals for UV LEDs which are employed for two users to transmit UV light. At the receiver side, a photomultiplier tube (PMT) is employed as the photon-detector, which is integrated with an optical filter and a sealed box. The UV signal of wavelength around 280nm can be detected, while the background radiation of other wavelengths is blocked. The PMT output signal is attenuated by an attenuator, amplified by an amplifier, and then filtered by a low-pass filter, which is then sampled by the oscilloscope. Finally, the photon counting processing, HMM-based MAP joint detection and decoding

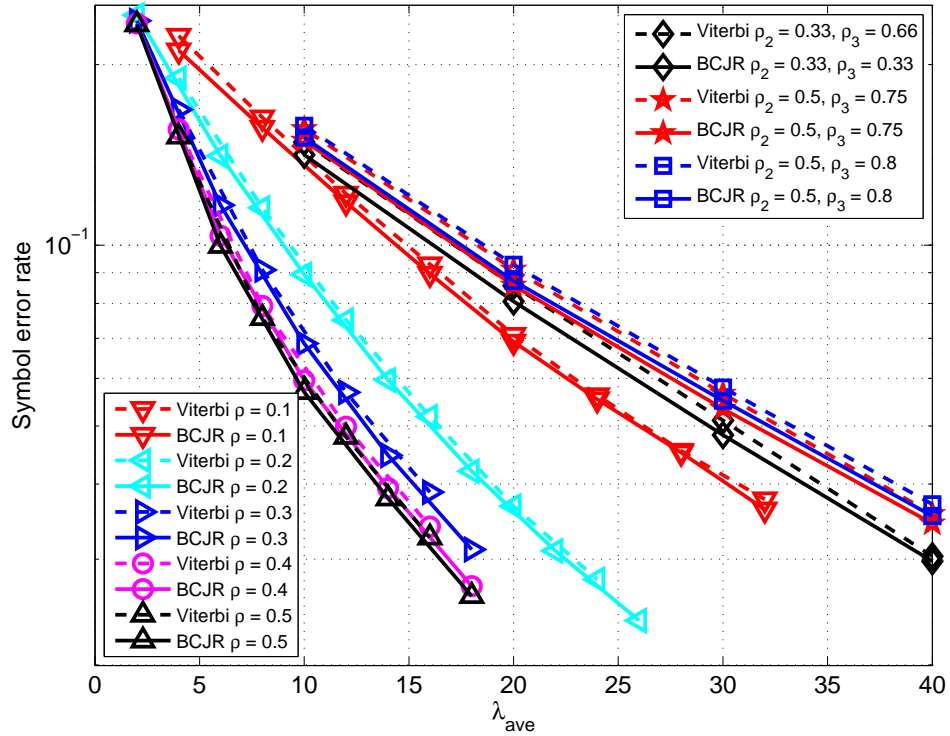


Fig. 8. The average symbol error rate of joint symbol detection for two-user and three-user AMA.

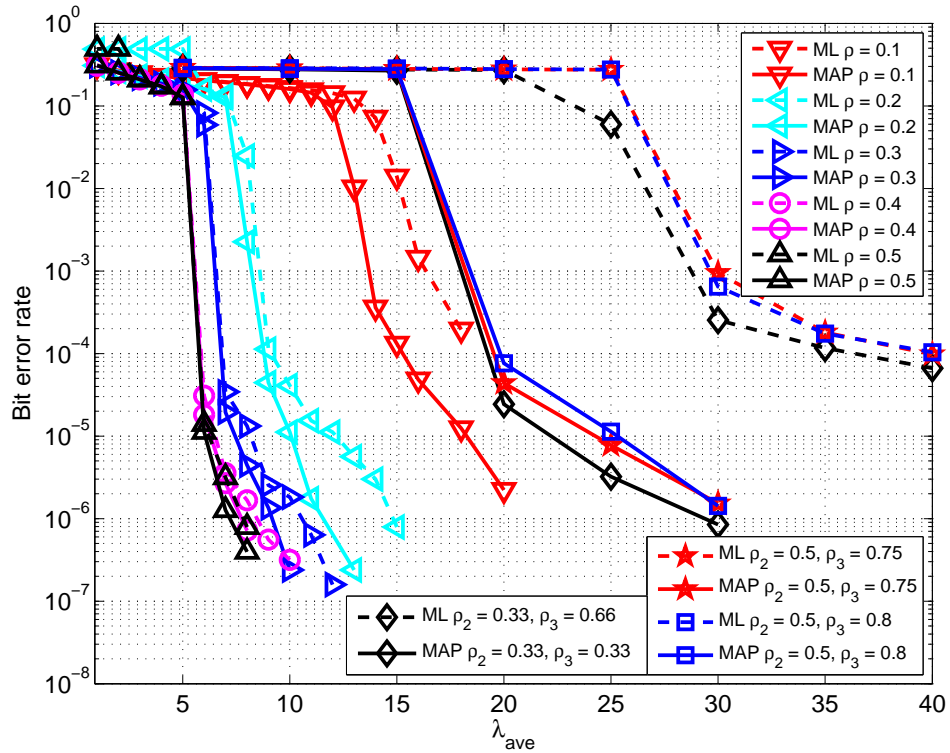


Fig. 9. The average bit error rate of joint detection and decoding with (12620, 6310) LDPC code.

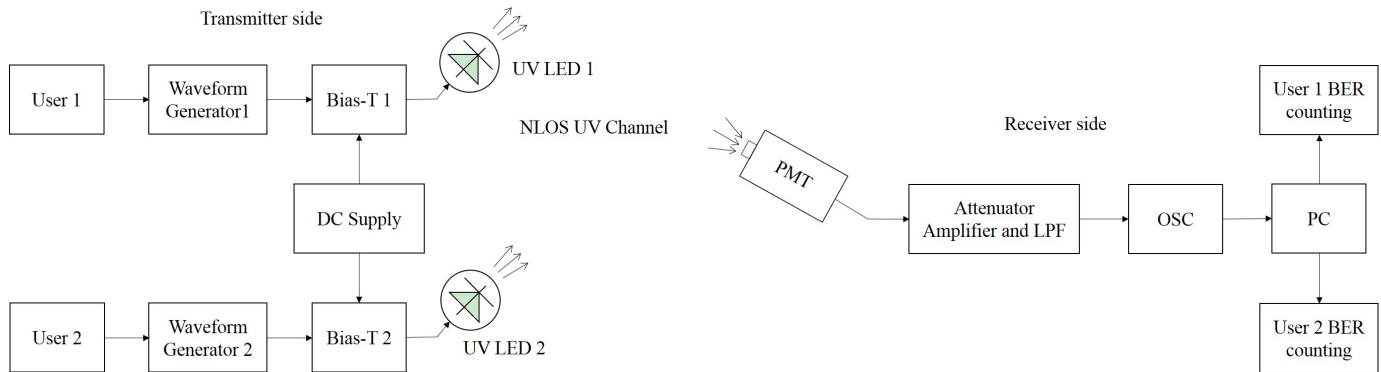


Fig. 10. Diagram of the experimental communication system for two user AMA UV communication.

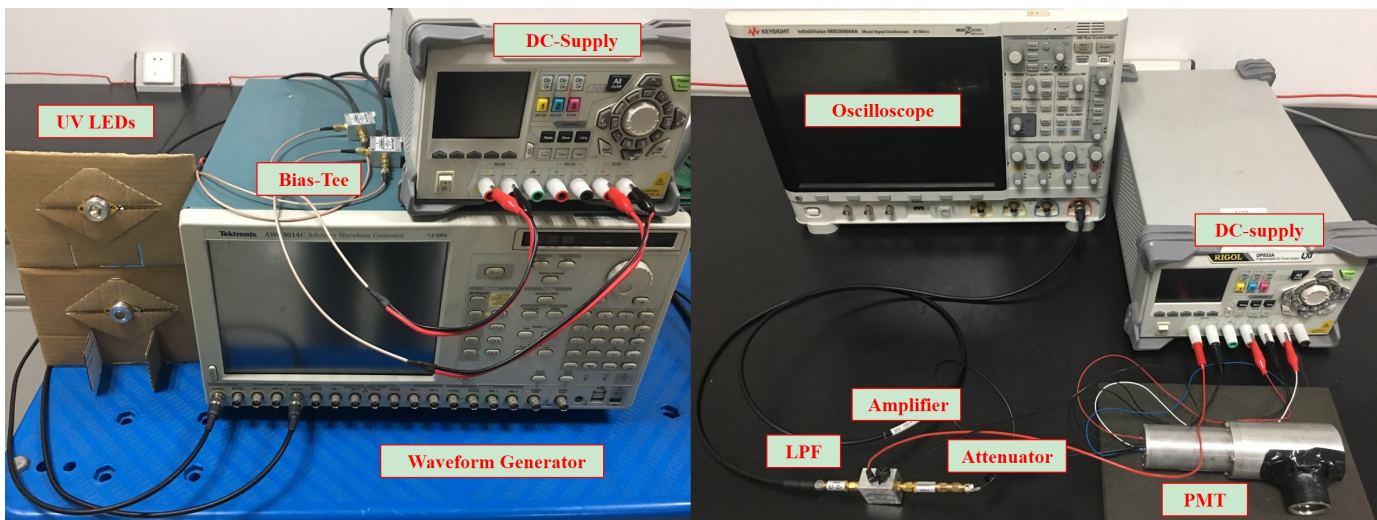


Fig. 11. Illustration of the transmitter-side (left) and receiver-side (right) test beds.

are realized in the received-side personal computer (PC) based on the sampled waveforms from the oscilloscope. Table I shows the specification of experimental device, and Figures 10 and 11 illustrate the entire experimental block diagram and the test bed realizations at transmitter and receiver sides, respectively.

TABLE I  
SPECIFICATION OF DEVICE FOR EXPERIMENT.

UV LED	Model	TO-3zz PO#2036
	Wavelength	280nm
Optical filter	Peak transmission	28.2%
	Aperture size	$\Phi 31.5\text{mm} \times 28.3\text{mm}$
PMT	Model	R7154
	Spectral response	160nm ~ 320nm
	Dark counts	< 10 per second
	Detection bandwidth	> 200MHz

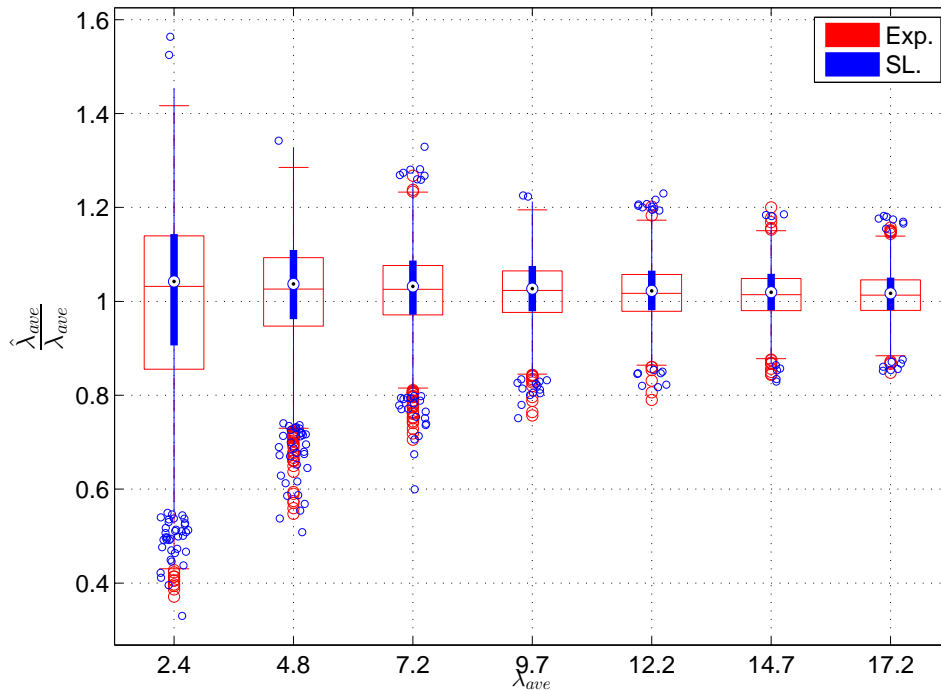


Fig. 12. Performance of EM-based channel estimation from simulation and experimental measurements.

In the experiments, the background radiation intensity is around 150 photoelectrons per second in the indoor environment. Furthermore, we hold the following conditions for two users: the symbol duration  $T_s = 1\mu s$ ; the same transmission power of the two LEDs leading to the approximately same average number of detected photoelectrons per bit  $\lambda_1 \approx \lambda_2 \triangleq \lambda_{ave}$ ; 2 different Gold-sequences as the pilots; the same parity check matrix construction and decoding algorithm of LDPC codes as those in simulation; and the uniform prior probabilities for 0 – 1 symbols. For each case of  $\lambda_{ave}$ , we count the bit error rate based on the transmission of  $1 \times 10^3$  frames ( $1.262 \times 10^7$  random bits).

Based on the experimental measurements, the performance of channel estimation, MAP detection with and without LDPC code (denoted as Exp.) are plotted in Figures 12, 13 and 14, respectively, where simulation results with identical channel parameters (denoted as SL.) are plotted for comparison. It is seen that as  $\lambda_{ave}$  grows, its variances decrease and the medians tend to approach the true value, which implies better performance of channel estimation for higher receiver side SNR. Moreover, the experimental results on the channel estimation, symbol detection and joint detection/decoding are close to the simulation results, where random  $\rho$  satisfies  $\rho \sim U(0, 1)$  in order to simulate the practical situation of 2 users' access. The above performance comparison shows the validity of the proposed channel estimation and signal detection approaches in real communication scenarios.

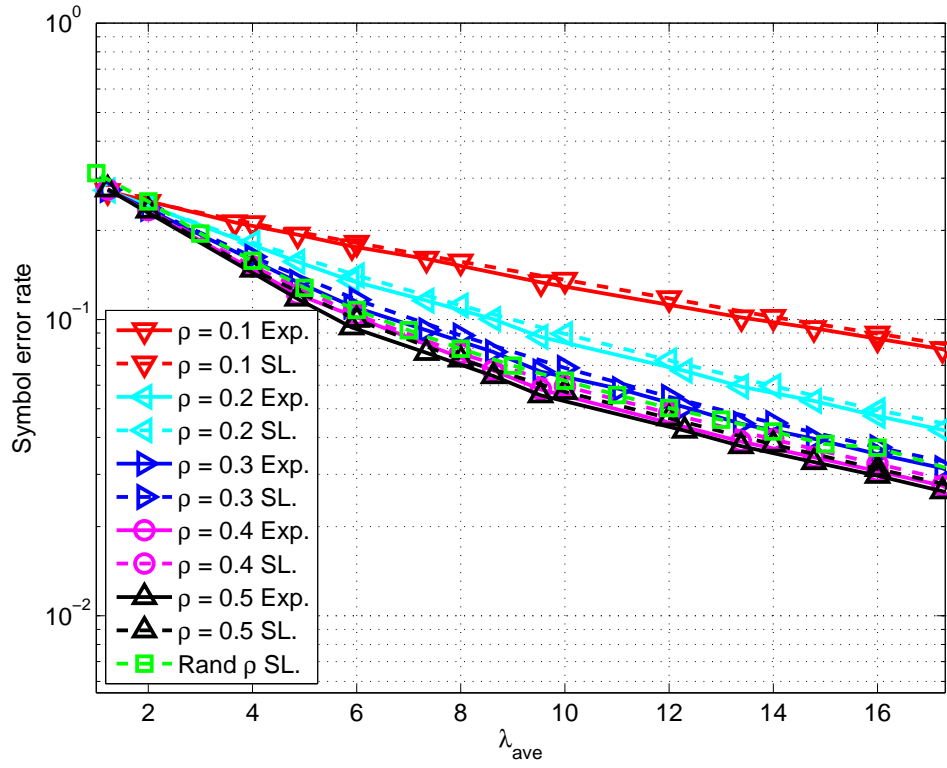


Fig. 13. The symbol error rate of proposed MAP detection for different relative delays  $\rho$  from simulation and experimental measurements.

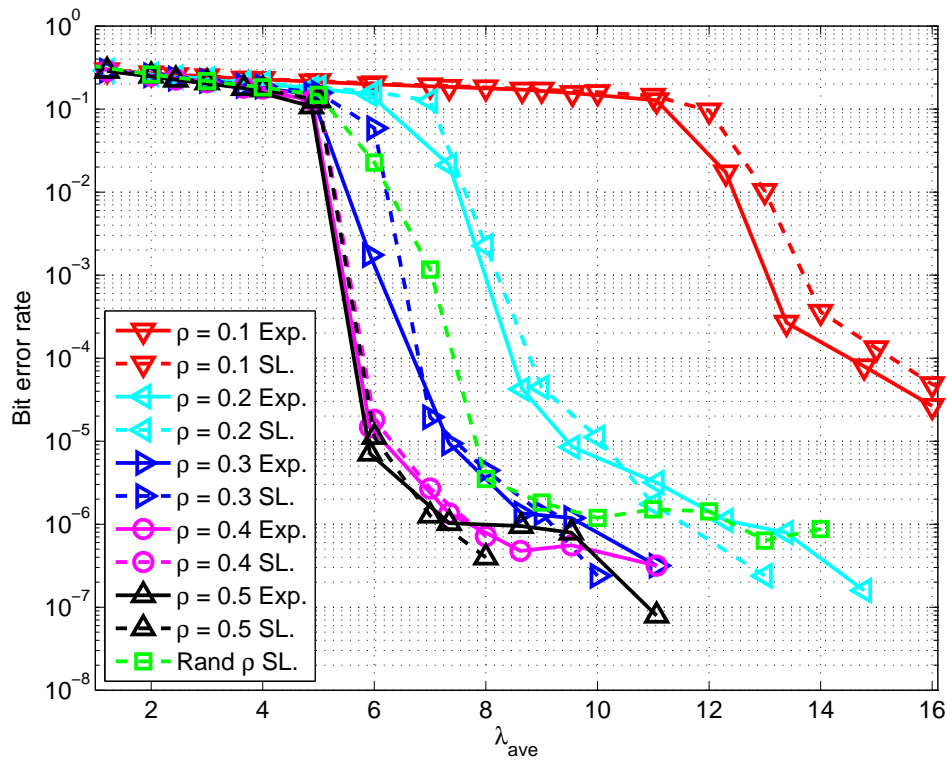


Fig. 14. The bit error rate of proposed MAP joint detection and decoding for different relative delays  $\rho$  from simulation and experimental measurements.

### VIII. CONCLUSION

We have proposed HMM-based model for discrete Poisson asynchronous multiple access channel. We have obtained the approximations on the achievable rates via Monte Carlo method. Moreover, we have proposed EM-based channel estimation and receiver-side AMA joint detection and decoding. The performance of the proposed receiver-side signal processing approaches is evaluated from both simulations and experiments. It is seen from both simulations and experiments that for two users case, the largest achievable rate and the lowest bit error rate for 2-user AMA are achieved when the receiver side SNRs of different users are nearly identical and  $\rho = 0.5$ .

### IX. APPENDIX

#### A. Proof of chain rules on conditional probabilities for two-user case

We prove the proposition based on the following chain rule on the probability of received signal given two users since the numbers of received photoelectrons in different chips are independent to each other,

$$\mathbb{P}(\mathbf{N}_T | \mathbf{Z}_1, \mathbf{Z}_2) = \prod_{t=1}^{\frac{T}{2}} \mathbb{P}(N_{2t-1} | Z_{1,t}, Z_{2,t}) \mathbb{P}(N_{2t} | Z_{1,t}, Z_{2,t+1}). \quad (43)$$

Consequently, Equation (21) can be proved by

$$\begin{aligned} \mathbb{P}(\mathbf{Z}_1 | \mathbf{Z}_2, \mathbf{N}_T) &= \mathbb{P}(Z_{1,1}, \mathbf{Z}_1^{[2,T/2]} | Z_{2,1}, Z_{2,2}, \mathbf{Z}_2^{[3,T/2+1]}, N_1, N_2, \mathbf{N}_{[3,T]}) \\ &= \frac{\mathbb{P}(Z_{1,1}, \mathbf{Z}_1^{[2,T/2]}, N_1, N_2, \mathbf{N}_{[3,T]} | Z_{2,1}, Z_{2,2}, \mathbf{Z}_2^{[3,T/2+1]})}{\sum_{Z_{1,1}} \sum_{\mathbf{Z}_1^{[2,T/2]}} \mathbb{P}(Z_{1,1}, \mathbf{Z}_1^{[2,T/2]}, N_1, N_2, \mathbf{N}_{[3,T]} | Z_{2,1}, Z_{2,2}, \mathbf{Z}_2^{[3,T/2+1]})} \\ &= \frac{\mathbb{P}(N_1 | Z_{1,1}, Z_{2,1}) \mathbb{P}(N_2 | Z_{1,1}, Z_{2,2}) \mathbb{P}(\mathbf{N}_{[3,T]} | \mathbf{Z}_1^{[2,T/2]}, Z_{2,2}, \mathbf{Z}_2^{[3,T/2+1]}) \mathbb{P}(Z_{1,1}) \mathbb{P}(\mathbf{Z}_1^{[2,T/2]})}{\sum_{Z_{1,1}} \sum_{\mathbf{Z}_1^{[2,T/2]}} \mathbb{P}(N_1 | Z_{1,1}, Z_{2,1}) \mathbb{P}(N_2 | Z_{1,1}, Z_{2,2}) \mathbb{P}(\mathbf{N}_{[3,T]} | \mathbf{Z}_1^{[2,T/2]}, Z_{2,2}, \mathbf{Z}_2^{[3,T/2+1]}) \mathbb{P}(Z_{1,1}) \mathbb{P}(\mathbf{Z}_1^{[2,T/2]})} \\ &= \frac{\mathbb{P}(N_1 | Z_{1,1}, Z_{2,1}) \mathbb{P}(N_2 | Z_{1,1}, Z_{2,2}) \mathbb{P}(Z_{1,1})}{\sum_{Z_{1,1}} \mathbb{P}(N_1 | Z_{1,1}, Z_{2,1}) \mathbb{P}(N_2 | Z_{1,1}, Z_{2,2}) \mathbb{P}(Z_{1,1})} \frac{\mathbb{P}(\mathbf{N}_{[3,T]} | \mathbf{Z}_1^{[2,T/2]}, Z_{2,2}, \mathbf{Z}_2^{[3,T/2+1]}) \mathbb{P}(\mathbf{Z}_1^{[2,T/2]})}{\sum_{\mathbf{Z}_1^{[2,T/2]}} \mathbb{P}(\mathbf{N}_{[3,T]} | \mathbf{Z}_1^{[2,T/2]}, Z_{2,2}, \mathbf{Z}_2^{[3,T/2+1]}) \mathbb{P}(\mathbf{Z}_1^{[2,T/2]})} \\ &= \frac{\mathbb{P}(Z_{1,1}, N_1, N_2 | Z_{2,1}, Z_{2,2})}{\sum_{Z_{1,1}} \mathbb{P}(Z_{1,1}, N_1, N_2 | Z_{2,1}, Z_{2,2})} \frac{\mathbb{P}(\mathbf{Z}_1^{[2,T/2]}, \mathbf{N}_{[3,T]} | Z_{2,2}, \mathbf{Z}_2^{[3,T/2+1]})}{\sum_{\mathbf{Z}_1^{[2,T/2]}} \mathbb{P}(\mathbf{Z}_1^{[2,T/2]}, \mathbf{N}_{[3,T]} | Z_{2,2}, \mathbf{Z}_2^{[3,T/2+1]})} \\ &= \mathbb{P}(Z_{1,1} | Z_{2,1}, Z_{2,2}, N_1, N_2) \mathbb{P}(\mathbf{Z}_1^{[2,T/2]} | \mathbf{Z}_2^{[2,T/2+1]}, \mathbf{N}_{[3,T]}) \\ &= \mathbb{P}(Z_{1,1} | Z_{2,1}, Z_{2,2}, N_1, N_2) \mathbb{P}(Z_{1,2} | Z_{2,2}, Z_{2,3}, N_3, N_4) \mathbb{P}(\mathbf{Z}_1^{[3,T/2]} | \mathbf{Z}_2^{[3,T/2+1]}, \mathbf{N}_{[5,T]}) \\ &= \prod_{t=1}^{\frac{T}{2}} \mathbb{P}(Z_{1,t} | Z_{2,t}, Z_{2,t+1}, N_{2t-1}, N_{2t}). \end{aligned} \quad (44)$$

Similar proof can be applied to  $\mathbb{P}(\mathbf{Z}_2 | \mathbf{Z}_1, \mathbf{N}_T)$  as well.  $\square$

### B. Proof of two users' conditional entropies

We prove the proposition by Equation (45) based on Proposition 1.

$$\begin{aligned}
H(\mathbf{Z}_1|\mathbf{Z}_2, N_T) &= \sum_{\mathbf{Z}_1, \mathbf{Z}_2 \in \mathcal{B}^{T/2}} \sum_{N_T \in \mathbb{N}^T} \mathbb{P}(N_T, \mathbf{Z}_1, \mathbf{Z}_2) \log_2 \mathbb{P}(\mathbf{Z}_1|\mathbf{Z}_2, N_T) \\
&= \sum_{\mathbf{Z}_1, \mathbf{Z}_2 \in \mathcal{B}^{T/2}} \mathbb{P}(\mathbf{Z}_1)\mathbb{P}(\mathbf{Z}_2) \sum_{N_T \in \mathbb{N}^T} \mathbb{P}(N_T|\mathbf{Z}_1, \mathbf{Z}_2) \log_2 \mathbb{P}(\mathbf{Z}_1|\mathbf{Z}_2, N_T) \\
&= \sum_{\mathbf{Z}_1, \mathbf{Z}_2 \in \mathcal{B}^{T/2}} \mathbb{P}(\mathbf{Z}_1)\mathbb{P}(\mathbf{Z}_2) \sum_{N_T \in \mathbb{N}^T} \prod_{t=1}^{T/2} \mathbb{P}(N_{2t-1}, N_{2t}|\mathbf{Z}_{1,t}, \mathbf{Z}_{2,t}, \mathbf{Z}_{2,t+1}) \sum_{t=1}^{T/2} \log_2 \mathbb{P}(\mathbf{Z}_{1,t}|\mathbf{Z}_{2,t}, \mathbf{Z}_{2,t+1}, N_{2t-1}, N_{2t}) \\
&= \sum_{t=1}^{T/2} \sum_{\mathbf{Z}_{1,t}, \mathbf{Z}_{2,t}, \mathbf{Z}_{2,t+1} \in \mathcal{B}} \mathbb{P}(\mathbf{Z}_{1,t})\mathbb{P}(\mathbf{Z}_{2,t})\mathbb{P}(\mathbf{Z}_{2,t+1}) \sum_{N_{2t-1}, N_{2t} \in \mathbb{N}} \mathbb{P}(N_{2t-1}, N_{2t}|\mathbf{Z}_{1,t}, \mathbf{Z}_{2,t}, \mathbf{Z}_{2,t+1}) \log_2 \mathbb{P}(\mathbf{Z}_{1,t}|\mathbf{Z}_{2,t}, \mathbf{Z}_{2,t+1}, N_{2t-1}, N_{2t}) \\
&= \frac{T}{2} \sum_{X, Y_1, Y_2 \in \mathcal{B}} \mathbb{P}(X)\mathbb{P}(Y_1)\mathbb{P}(Y_2) \sum_{N_1, N_2 \in \mathbb{N}} \mathbb{P}(N_1, N_2|X, Y_1, Y_2) \log_2 \mathbb{P}(X|Y_1, Y_2, N_1, N_2) \\
&= \frac{T}{2} \sum_{X, Y_1, Y_2 \in \mathcal{B}} \mathbb{P}(X)\mathbb{P}(Y_1)\mathbb{P}(Y_2) \sum_{N_1, N_2 \in \mathbb{N}} \mathbb{P}(N_1|X, Y_1)\mathbb{P}(N_2|X, Y_2) \log_2 \frac{\mathbb{P}(N_1|X, Y_1)\mathbb{P}(N_2|X, Y_2)\mathbb{P}(X)}{\sum_{X \in \mathcal{B}} \mathbb{P}(X)\mathbb{P}(N_1|X, Y_1)\mathbb{P}(N_2|X, Y_2)}
\end{aligned} \tag{45}$$

The proof can also be applied to  $H(\mathbf{Z}_2|\mathbf{Z}_1, N_T)$ . □

### C. Proofs of M-step and Convergency of Estimation Algorithm

The likelihood function is given by

$$\begin{aligned}
\mathcal{L}(N_t|\lambda_{s_i} = \hat{\lambda}_{s_i}^{(v)}) &= \sum_{t=1}^{T'} \log \sum_{s_i \in \mathcal{B}^{K'}} \mathbb{P}(N_t, \mathbf{S}_t = s_i|\lambda_{s_i} = \hat{\lambda}_{s_i}^{(v)}) \\
&\geq \sum_{t=1}^{T'} \sum_{s_i \in \mathcal{B}^{K'}} Q^{(v)}(\mathbf{S}_t = s_i) \log \frac{\mathbb{P}(N_t, \mathbf{S}_t = s_i|\lambda_{s_i} = \hat{\lambda}_{s_i}^{(v)})}{Q^{(v)}(\mathbf{S}_t = s_i)}.
\end{aligned} \tag{46}$$

Letting  $\tilde{\mathcal{L}}^{(v)}(N_t|\lambda_{s_i} = \hat{\lambda}_{s_i}^{(v)})$  denote the last term of above inequality, we have that

$$\tilde{\mathcal{L}}^{(v)}(N_t|\lambda_{s_i} = \hat{\lambda}_{s_i}^{(v)}) \sim \sum_{t=1}^{T'} \sum_{s_i \in \mathcal{B}^{K'}} Q^{(v)}(\mathbf{S}_t = s_i) \sum_{m=1}^W \left[ N_{t,m} \log \frac{\tau_t \hat{\lambda}_{s_i}^{(v)}}{W} - \log N_{t,m}! - \frac{\tau_t \hat{\lambda}_{s_i}^{(v)}}{W} \right].$$

Hence the partial derivative of likelihood function is given by

$$\frac{\partial}{\partial \lambda_{s_i}^{(v)}} \tilde{\mathcal{L}}^{(v)}(N_t = \mathbf{n}_t|\lambda_{s_i} = \hat{\lambda}_{s_i}^{(v)}) = \sum_{t=1}^{T'} Q^{(v)}(\mathbf{S}_t = s_i) \left[ \frac{1}{\hat{\lambda}_{s_i}^{(v)}} \sum_{m=1}^W N_{t,m} - \sum_{m=1}^W \frac{\tau_t}{W} \right]. \tag{47}$$

Letting  $\frac{\partial}{\partial \lambda_{s_j}^{(v)}} \mathcal{L}(N_t = \mathbf{n}_t|\lambda_{s_j} = \hat{\lambda}_{s_j}^{(v)}) = 0$ , we have that

$$\hat{\lambda}_{s_j}^{(v)} = \arg \max \tilde{\mathcal{L}}^{(v)}(N_t = \mathbf{n}_t|\lambda_{s_i} = \hat{\lambda}_{s_i}^{(v)}) = \frac{\sum_{t=1}^{T'} Q^{(v)}(\mathbf{S}_t = s_i) \sum_{m=1}^W N_{t,m}}{\sum_{t=1}^{T'} Q^{(v)}(\mathbf{S}_t = s_i) \tau_t}. \tag{48}$$

According to Equations (46) and (48), we have  $\mathcal{L}(N_t|\lambda_{s_i} = \hat{\lambda}_{s_i}^{(v)}) \geq \tilde{\mathcal{L}}^{(v)}(N_t = \mathbf{n}_t|\lambda_{s_i} = \hat{\lambda}_{s_i}^{(v)})$  and  $\tilde{\mathcal{L}}^{(v)}(N_t = \mathbf{n}_t|\lambda_{s_i} = \hat{\lambda}_{s_i}^{(v)}) \geq \tilde{\mathcal{L}}^{(v)}(N_t = \mathbf{n}_t|\lambda_{s_i} = \hat{\lambda}_{s_i}^{(v-1)})$ . Furthermore, we have the following proof on  $\tilde{\mathcal{L}}^{(v)}(N_t|\lambda_{s_i} = \hat{\lambda}_{s_i}^{(v-1)}) = \mathcal{L}(N_t|\lambda_{s_i} = \hat{\lambda}_{s_i}^{(v-1)})$ ,

$$\begin{aligned}
\tilde{\mathcal{L}}^{(v)}(N_t|\lambda_{s_i} = \hat{\lambda}_{s_i}^{(v-1)}) &= \sum_{t=1}^{T'} \sum_{s_i \in \mathcal{B}^{K'}} Q^{(v)}(\mathbf{S}_t = \mathbf{s}_i) \log \frac{\mathbb{P}(N_t, \mathbf{S}_t = \mathbf{s}_i|\lambda_{s_i} = \hat{\lambda}_{s_i}^{(v-1)})}{Q^{(v)}(\mathbf{S}_t = \mathbf{s}_i)} \\
&= \sum_{t=1}^{T'} \sum_{s_i \in \mathcal{B}^{K'}} \mathbb{P}(\mathbf{S}_t = \mathbf{s}_i|N_t, \lambda_{s_i} = \hat{\lambda}_{s_i}^{(v-1)}) \log \frac{\mathbb{P}(N_t, \mathbf{S}_t = \mathbf{s}_i|\lambda_{s_i} = \hat{\lambda}_{s_i}^{(v-1)})}{\mathbb{P}(\mathbf{S}_t = \mathbf{s}_i|N_t, \lambda_{s_i} = \hat{\lambda}_{s_i}^{(v-1)})} \\
&= \sum_{t=1}^{T'} \sum_{s_i \in \mathcal{B}^{K'}} \mathbb{P}(\mathbf{S}_t = \mathbf{s}_i|N_t, \lambda_{s_i} = \hat{\lambda}_{s_i}^{(v-1)}) \log \mathbb{P}(N_t|\lambda_{s_i} = \hat{\lambda}_{s_i}^{(v-1)}) \\
&= \sum_{t=1}^{T'} \log \mathbb{P}(N_t|\lambda_{s_i} = \hat{\lambda}_{s_i}^{(v-1)}) \\
&= \mathcal{L}(N_t|\lambda_{s_i} = \hat{\lambda}_{s_i}^{(v-1)}).
\end{aligned} \tag{49}$$

Consequently,  $\mathcal{L}(N_t|\lambda_{s_i} = \hat{\lambda}_{s_i}^{(v)}) \geq \mathcal{L}(N_t|\lambda_{s_i} = \hat{\lambda}_{s_i}^{(v-1)})$ , i.e.,  $\hat{\Lambda}_T^{(v)}$  is closer to the value of ML estimation than  $\hat{\Lambda}_T^{(v-1)}, \hat{\Lambda}_T^{(v-2)}, \dots, \hat{\Lambda}_T^{(1)}$ .

## REFERENCES

- [1] Z. Xu and B. M. Sadler, "Ultraviolet communications: potential and state-of-the-art," *IEEE Commun. Mag.*, vol. 46, no. 5, May 2008.
- [2] C. Xu, H. Zhang, and J. Cheng, "Effects of haze particles and fog droplets on NLOS ultraviolet communication channels," *Opt. Express*, vol. 23, no. 18, pp. 23259–23269, 2015.
- [3] Y. Sun and Y. Zhan, "Closed-form impulse response model of non-line-of-sight single-scatter propagation," *JOSA A*, vol. 33, no. 4, pp. 752–757, 2016.
- [4] N. Raptis, E. Pikasis, and D. Syvridis, "Power losses in diffuse ultraviolet optical communications channels," *Opt. Lett.*, vol. 41, no. 18, pp. 4421–4424, 2016.
- [5] M. Davis, "Capacity and cutoff rate for Poisson-type channels," *IEEE Trans. Inform. Theory*, vol. 26, no. 6, pp. 710–715, Jun. 1980.
- [6] A. D. Wyner, "Capacity and error exponent for the direct detection photon channel. I-II," *IEEE Trans. Inform. Theory*, vol. 34, no. 6, pp. 1449–1461, Jun. 1988.
- [7] M. R. Frey, "Information capacity of the Poisson channel," *IEEE Trans. Inform. Theory*, vol. 37, no. 2, pp. 244–256, Feb. 1991.
- [8] A. Lapidoth and S. M. Moser, "On the capacity of the discrete-time Poisson channel," *IEEE Trans. Inform. Theory*, vol. 55, no. 1, pp. 303–322, Jan. 2009.
- [9] A. Lapidoth, J. H. Shapiro, V. Venkatesan, and L. Wang, "The discrete-time Poisson channel at low input powers," *IEEE Trans. Inform. Theory*, vol. 57, no. 6, pp. 3260–3272, Jun. 2011.
- [10] J. Cao, S. Hranilovic, and J. Chen, "Capacity-achieving distributions for the discrete-time Poisson channel Part I-II: General properties and numerical techniques," *IEEE Trans. Commun.*, vol. 62, no. 1, pp. 194–202, 203–213, Jan. 2014.
- [11] N. Mehravari and T. Berger, "Poisson multiple-access contention with binary feedback," *IEEE Trans. Inform. Theory*, vol. 30, no. 5, pp. 745–751, May 1984.

- [12] A. Lapidoth and S. Shamai, "The Poisson multiple-access channel," *IEEE Trans. Inform. Theory*, vol. 44, no. 2, pp. 488–501, Feb. 1998.
- [13] S. I. Bross, M. V. Burnashev, and S. Shamai, "Error exponents for the two-user Poisson multiple-access channel," *IEEE Trans. Inform. Theory*, vol. 47, no. 5, pp. 1999–2016, May 2001.
- [14] G. Wang, C. Gong, and Z. Xu, "Signal detection and achievable rates for multiple access optical wireless scattering communication," *IEEE Global Communications Conference*, Dec. 4–7, 2017.
- [15] L. Rabiner and B. Juang, "An introduction to hidden Markov models," *IEEE ASSP Mag.*, vol. 3, no. 1, pp. 4–16, Jun. 1986.
- [16] S. R. Eddy, "Hidden markov models," *Current opinion in structural biology*, vol. 6, no. 3, pp. 361–365, Jun. 1996.
- [17] Y. Ephraim and N. Merhav, "Hidden markov processes," *IEEE Trans. Inform. Theory*, vol. 48, no. 6, pp. 1518–1569, Jun. 2002.
- [18] T. K. Moon, "The expectation-maximization algorithm," *IEEE Signal Processing Mag.*, vol. 13, no. 6, pp. 47–60, Nov. 1996.
- [19] G. McLachlan and T. Krishnan, *The EM Algorithm and Extensions*, vol. 382. John Wiley & Sons, 2007.
- [20] G. D. Forney, "The viterbi algorithm," *Proc. IEEE*, vol. 61, no. 3, pp. 268–278, Mar. 1973.
- [21] J. Hagenauer and P. Hoeher, "A Viterbi algorithm with soft-decision outputs and its applications," *IEEE Global Communications Conference*, Nov. 27–30, 1989.
- [22] L. Bahl, J. Cocke, F. Jelinek, and J. Raviv, "Optimal decoding of linear codes for minimizing symbol error rate (corresp.)," *IEEE Trans. Inform. Theory*, vol. 20, no. 2, pp. 284–287, Feb. 1974.
- [23] P. Robertson, E. Villebrun, and P. Hoeher, "A comparison of optimal and sub-optimal MAP decoding algorithms operating in the log domain," *IEEE International Conference on Communications*, Jun. 18–22, 1995.
- [24] J. Hagenauer, E. Offer, and L. Papke, "Iterative decoding of binary block and convolutional codes," *IEEE Trans. Inform. Theory*, vol. 42, no. 2, pp. 429–445, Feb. 1996.
- [25] S. Benedetto, D. Divsalar, G. Montorsi, and F. Pollara, "A soft-input soft-output APP module for iterative decoding of concatenated codes," *IEEE Commun. Lett.*, vol. 1, no. 1, pp. 22–24, Jan. 1997.
- [26] D. Hernando, V. Crespi, and G. Cybenko, "Efficient computation of the hidden Markov model entropy for a given observation sequence," *IEEE Trans. Inform. Theory*, vol. 51, no. 7, pp. 2681–2685, Jul. 2005.
- [27] X. Liu, C. Gong, S. Li, and Z. Xu, "Signal characterization and receiver design for visible light communication under weak illuminance," *IEEE Commun. Lett.*, vol. 20, no. 7, pp. 1349–1352, Jul. 2016.
- [28] M. Yang, W. E. Ryan, and Y. Li, "Design of efficiently encodable moderate-length high-rate irregular LDPC codes," *IEEE Trans. Commun.*, vol. 52, no. 4, pp. 564–571, Apr. 2004.
- [29] M. P. Fossorier, "Quasicyclic low-density parity-check codes from circulant permutation matrices," *IEEE Trans. Inform. Theory*, vol. 50, no. 8, pp. 1788–1793, Aug. 2004.
- [30] J. Chen, A. Dholakia, E. Eleftheriou, M. P. Fossorier, and X.-Y. Hu, "Reduced-complexity decoding of LDPC codes," *IEEE Trans. Commun.*, vol. 53, no. 8, pp. 1288–1299, Aug. 2005.